Optical Spectroscopy of Single Nanowires

Trägårdh, Johanna

2008

Optical spectroscopy of single nanowires

Johanna Trägårdh

LUND
UNIVERSITY

Department of Physics
Lund, Sweden 2008

Akademisk avhandling för avläggande av teknologie doktorsexamen vid tekniska fakulteten vid Lunds universitet. Avhandlingen kommer att offentligen försvaras fredagen den 13 juni 2008 kl. 10.15, hörsal B, Fysiska Institutionen, Sölvegatan 14. Fakultetsopponent: Dr. Heike Riel, IBM, Zurich Research Laboratory, Rüschlikon, Schweiz

Division of Solid State Physics
Department of Physics
Lund University
P.O. Box 118
SE-221 00 Lund
Sweden

ISBN 978-91-628-7510-7
Printed in Sweden by Media-Tryck, Lund
May 2008

Abstract

This thesis describes optical spectroscopy on III-V semiconductor nanowires. The nanowires were grown by metal-organic vapor phase epitaxy (MOVPE) and chemical beam epitaxy (CBE). Photoluminescence and photocurrent spectroscopy are used as tools to investigate issues such as the size of the band gap, the effects of surface states, and the charge carrier transport in core-shell nanowires.

The band gap of $InAs_{1-x}P_x$ nanowires with wurtzite crystal structure is measured as a function of the composition for $0.15 < x < 0.48$. The band gap is measured using photocurrent spectroscopy on single InAs nanowires with a centrally placed $InAs_{1-x}P_x$ segment. The wurtzite band gap is found to be about 120 meV larger than the corresponding zinc blende band gap over the entire composition range. The photocurrent spectrum is measured for excitation polarized parallel and perpendicular to the nanowire axis. The nanowires are found to have a large polarization dependence of the photocurrent, which is explained by the difference in dielectric constant of the nanowire and the surrounding air. The large polarization dependence in combination with the tunable band gap and the low dark current due to the band edge offset in the heterostructure, makes such nanowires possible candidates for polarization-sensitive photodetectors in the infrared.

The effect on the optical properties of the crystal structure is further investigated by comparing the spectral excitation power dependence of InP nanowires with zinc blende crystal structure and InP nanowires with a high density of rotational twins. The difference in excitation power dependence is explained by interpreting the rotational twins as monolayer thick wurtzite segments. The rotationally twinned structure responds to the light as a type II heterostructure due to the type II offset between the zinc blende and wurtzite energy bands.

p- and *n*-doped InP nanowires are studied with photoluminescence spectroscopy. The radial band bending caused by the Fermi level pinning at the surface, causes the electrons and holes to be separated radially and this is observed as a lowering of the photoluminescence energy. This is further in-

vestigated by applying a gate voltage on the nanowire sample to change the band bending, and observe the changes in the photoluminescence signal. This could potentially be used for investigating the doping concentration in such nanowires.

Core-shell nanowires with GaAs core and a larger band gap $Ga_xIn_{1-x}P$ shell are studied by photoluminescence and time-resolved photoluminescence spectroscopy. It is observed that the photoluminescence decay is fast, indicating that the decay is dominated by non-radiative recombination also with a passivating shell on the nanowire. The charge carrier transport from the shell to the core is partially hindered at the low temperatures used (10 K). The photoluminescence decay is modelled by simple rate equations, with qualitative agreement with the experiments. It is also studied how the strain from the lattice mismatched shell, and the choice of substrate (Si or GaP) affects the photoluminescence intensity and decay time. It is found that the maximum PL intensity is obtained for unstrained nanowires.

A smaller part of the thesis describes photoluminescence measurements on the conjugated polymer MEH-PPV (poly[2-methoxy-5-(2'-ethyl-hexyloxy)-1,4-phenylene vinylene]). The measurements are performed on single polymer chains dispersed in a PMMA matrix. The polymer spectra acquired at room temperature and 20 K are compared to obtain information about the conformational dynamics of the polymer chain. It is observed that at 20 K, the photoluminescence spectrum has a narrow line width and there is a large spread in the distribution of the spectral maxima. This was explained by assuming that at this low temperature, the thermal energy was not enough to allow conformational changes, and each single chain is frozen in a specific conformation. At room temperature conformational changes are possible, resulting in the single chain spectra being broad with only small inhomogeneous broadening of the ensemble spectrum.

List of papers

This thesis is based on the following papers, which will be referred to in the text by their Roman numerals. The papers are appended at the end of the thesis.

I. Temperature effect on single chain MEH-PPV spectra
C. Rønne, J. Trägårdh, D. Hessman, V. Sundström
Chem. Phys. Lett. **388**, 40 (2004)

II. Growth and optical properties of strained GaAs-$Ga_xIn_{1-x}P$ core-shell nanowires
N. Sköld, L.S. Karlsson, M.W. Larsson, M-E Pistol, W. Seifert, J. Trägårdh, L. Samuelson
Nano Letters **5**, 1943 (2005)

III. Infrared Photodetectors in Heterostructure Nanowires
H. Pettersson, J. Trägårdh, A.I. Persson, L. Landin, D. Hessman, L. Samuelson
Nano Letters **6**, 229 (2006)

IV. Measurements of the band gap of wurtzite $InAs_{1-x}P_x$ nanowires using photocurrent spectroscopy
J. Trägårdh, A.I. Persson, J.B. Wagner, D. Hessman, L. Samuelson
Journal of Applied physics **101**, 123701 (2007)

V. Optical Properties of Rotationally Twinned InP Nanowires
J. Bao, D. C. Bell, F. Capasso, J. B. Wagner, T. Mårtensson, J. Trägårdh and L. Samuelson
Nano Letters **8** 836 (2008)

VI. Monolithic GaAs/InGaP nanowire LEDs on silicon
P. Svensson, T. Mårtensson, J. Trägårdh, C. Larsson, M. Rask, D. Hessman, L. Samuelson, J. Ohlsson
Submitted to Nanotechnology (2008)

VII. Gate-dependent photoluminescence from single *p*- and *n*-doped InP nanowires
J. Trägårdh, D. Hessman, M.T. Borgström, E. Norberg and L. Samuelson
Manuscript (2008)

The following paper is not incuded in the thesis
viii. Investigations of InAs surface dots on InP
C. Ellström, J. Trägårdh, L. Samuelson, W. Seifert, M-E. Pistol, S. Lemeshko and C. Pryor
Appl. Phys. Lett. **89** 033111 (2006)

Preface

The work presented in this thesis was performed during the years 2003–2008 at the division of Solid State Physics at Lund University. The thesis deals mainly with optical spectroscopy on III-V semiconductor nanowires. Photoluminescence and photocurrent spectroscopy are used as tools to investigate issues such as the size of the band gap, the occurrence and effects of surface states, the charge carrier transport in core-shell nanowires and the optical effects of twin defects in the crystal. The spectroscopy is mostly done on single nanowires. A smaller part of the thesis is related to photoluminescence spectroscopy on the conjugated polymer MEH-PPV, with the purpose of investigating the conformational dynamics (the folding and refolding) of the polymer.

The thesis is organized in six chapters, providing a background to, and further discussing the results presented in the papers. The seven papers are appended at the end of the thesis. The first chapter serves as a brief introduction to nano and nanowires, with a focus on optical properties. Chapter 2 introduces the experimental methods used in this thesis, namely photoluminescence, time-resolved photoluminescence and photocurrent spectroscopy. It also describes the measurement setups and the fabrication of the samples. Chapter 3 discusses how the radial band bending induced by Fermi level pinning at the nanowire surface affects the photoluminescence. This is related primarily to the work in Paper VII. Chapter 4 discusses photoluminescence measurements on core-shell nanowires, related to Papers II and VI. In Chapter 5 the crystal structure of the nanowires is discussed, focusing on the effects of the possibility for these nanowires to grow as both wurtzite and zinc blende. The presented results are from measurements on nanowires in the InAsP material system, related to Papers III, IV and V. Chapter 6 provides a background to Paper I, which discusses single molecule spectroscopy on the conjugated polymer MEH-PPV. It also gives a brief introduction to conjugated polymers in general.

There are a number of people who have contributed to this thesis in various ways (and I'm sure I will forget to mention at least some of you, I

apologize for that):

I would like to thank my supervisor Prof. Lars Samuelson. Lars is always very enthusiastic about research, and a seemingly endless source of new exciting ideas and projects (although some of them might not be possible to currently realize in the lab). He always somehow finds the time to have relevant input on research projects and manuscripts.

The second supervisor, and the person actually doing most of the supervision is Dan Hessman. Dan has been a valuable source of knowledge about all sorts of technical stuff in the PL-lab. I would also like to thank Dan for his patience and for the long, but interesting, discussions about the research projects.

I would also like to thank those who provided the sample material for this research: The nanowires were grown by Ann Persson, Niklas Sköld, Thomas Mårtensson, and Jessica Eriksson. The MEH-PPV was provided by M. Johansson and M. Anderson, Dept. Polymer Technology, Chalmers University of Technology

Håkan Pettersson and Lars Landin are acknowledged for teaching me how to run the Fourier transform spectrometer, and for collaboration on the project on wurtzite InAsP.

Lena Timby, Mariusz Graczyk, Ivan Maximov, and David Adolph are acknowledge for teaching me a lot of processing and helping out with fabricating substrates, evaporation etc.

I wish to thank Cecilie Rønne for support and for her great enthusiasm during the project with the conjugated polymers. I would also like to thank the other researchers in the group of Prof. Villy Sundström at Chemical Physics for lots of interesting discussions about the conjugated polymers.

A big thanks to Sara Ghatnekar-Nilsson for encouraging me and for many insightful comments and advises about the part of the research that is not directly related to the labwork.

Ann Persson is acknowledged for the collaboration during the wurtzite InAsP project. Ann; It was great fun to work with you, and thanks for all the (also project non-related) support.

The optics group would definitely be less fun without Mats-Erik Pistol. Mats-Erik is also acknowledged for relevant and interesting input on the more theoretical aspects of the research field. I also want to thank the other (former and preset) members of the group, Ulf, Carl, Jonas, Niki, Anders, Zeila, for nice collaboration. In particular Niklas for all the samples and the collaboration on the core-shell nanowire project.

Thanks to Carina Fasth, Jessica Eriksson, Monica Lexholm and Niklas Sköld for critically reading and commenting on the thesis. Carina: thanks

for being a fun room-mate during these years.

I want to thank Andreas Ollén for lots of encouragement.

Finally, I am grateful for the support from my mother and my brother.

Lund, May 2008

Johanna Trägårdh

Contents

Chapter 1

Introduction

Nanoscience is an interdisciplinary research field, spanning biology and chemistry as well as physics disciplines such as electronics, optics and mechanics, which deals with structures in the size range 1–100 nm and phenomena occurring in such structures. Two things characterize objects at this length scale; the surface to volume ratio is very large, so that the structure is highly sensitive to the quality and properties of the surface, and the dimensions are on the order of the wavelength of the electron, so that quantum mechanical effects such as energy quantization and tunneling become important.

The nanoscale objects studied in this thesis are III-V semiconductor nanowires. Nanowires are structures with a lateral size on the order of 100 nm and a length much larger than the thickness. The nanowires studied here are epitaxially grown free standing on a surface, (i.e. they are not embedded in semiconductor material). The diameter and the length, as well as the chemical composition [1, 2] of the nanowire can be controlled, and it is also possible to change the material during growth to fabricate heterostructures inside the nanowire [3], [4], [5].

One of the most interesting features of such freestanding nanowires is the possibility to grow heterostructure with material combinations not possible in bulk due to a large lattice mismatch. This advantage comes from their small lateral dimension allowing strain to relax radially [6]. From an optics point of view, it is highly desirable to integrate the direct band gap III-V materials, that are efficient light emitters, on Si [7]. Nanowires can be one route to achieve this, since their ability to radially relax strain can be used to overcome the problems with the large lattice mismatch, as well as a difference in thermal expansion coefficient between Si and III-V materials, and light emitting nanowire structures grown on Si have been demonstrated [8, 9] [Paper VI].

The large surface to volume ratio of nanowires, and nanostructures in general, is an advantage for applications such as sensors and catalysis where the surface is the active area. For many optics applications, however, the surface constitutes a problem due to the large number of surface states. These surface states are often non-radiative recombination centers, and thus they reduce the light emission efficiency. Furthermore, the surface states pin the Fermi level, which induces a band bending and depletes a large fraction of the nanowire of free carriers.

These problems with the surface can be at least partially overcome by growth of a larger band gap shell on the nanowire. The surface is thereby separated from the charge carriers confined in the nanowire core. Such core-shell structures has been studied both for the passivating effect of the shell [10–12], [Paper II], and for devices based on radial heterostructures [13–16] [Paper VI]. In this thesis, the passivating effect of the shell is studied for GaAs-GaInP core-shell nanowires, using time-resolved photoluminescence (PL) spectroscopy. Furthermore, the effect of strain induced by the nanowire shell on the PL intensity from the core is studied.

Another issue that needs to be addressed for nanowires is the crystal structure. Whereas most bulk III-V semiconductors have a zinc blende crystal structure, the nanowires can be both zinc blende and wurtzite. Nanowires with [111]B growth direction, which is the most commonly observed growth direction [17], exhibit rotational twinning, and since the twin interface in a zinc blende crystal can be interpreted as a monolayer with wurtzite symmetry, the crystal structure is effectively alternating between zinc blende and wurtzite. Due to the difference in crystal symmetry, the two crystal structures have different material parameters such as band gap, band offsets and effective masses. A mixed wurtzite-zinc blende crystal structure therefore results in a non-intentional heterostructure along the nanowire axis. In Paper IV the band gap of wurtzite $InAs_{1-x}P_x$ nanowires is measured with photocurrent spectroscopy and Paper V presents results from measurements of the effects of the rotationally twinned crystal structure on the excitation power dependence of PL from InP nanowires.

Chapter 2

Methods

The interaction of light with a semiconductor provides information about the band structure as well as the dynamics of the charge carriers via the energy, the polarization and the time dependence of the emitted or absorbed light. A large number of methods based on light-matter interaction in the form of emission, absorption and scattering exist, and the methods used to characterize the nanowires and molecules in this thesis are photoluminescence and photocurrent spectroscopy. This chapter describes these techniques as well as the experimental setups used.

2.1 Photoluminescence spectroscopy

In a photoluminescence (PL) experiment electrons and holes are created by optical excitation. The optically generated electrons and holes rapidly thermalize and relax to the band edge. The charge carriers can also diffuse in the semiconductor material and transfer across heterostructure interfaces, such as from the large band gap shell to the low band gap core in a core-shell nanowire. The electrons and holes can then either recombine radiatively across the band gap, and via energy states in the band gap such as dopants, giving rise to luminescence, or recombine non-radiatively, via lower lying (midgap) energy levels in the band gap, for example surface states. The recombination processes are illustrated in Figure 2.1. For a nanowire, where the surface to volume ratio is very large and the carriers are close to the surface, the surface states are important non-radiative recombination centers. Since non-radiative recombination processes compete with the radiative recombination for the charge carriers, the number of non-radiative recombination possibilities should be reduced for an efficient light emission. This requires surface passivation and a crystal of high quality, without defects and stack-

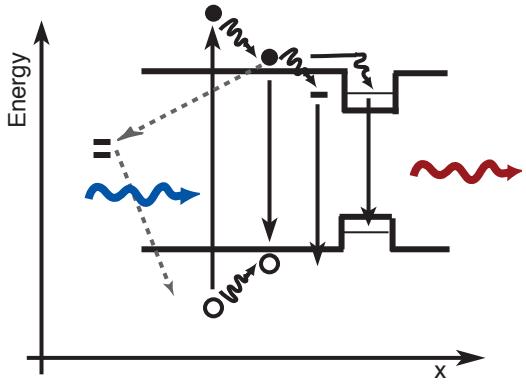

Figure 2.1: Optical excitation and recombination processes in a semiconductor. The figure illustrates the relaxation of charge carriers (the thin wavy arrows) and the radiative recombination across the band gap and via energy states in the band gap (straight arrows). The non-radiative recombination via surface states is indicated by dashed arrows.

ing faults. One method to further study the recombination processes and the charge carrier dynamics is time-resolved PL, which is described below.

2.1.1 Time-resolved photoluminescence

In a time-resolved PL experiment the sample is excited with a short pulse of light and the emission is studied as a function of the time that has passed since the excitation. The PL intensity is a measure of the rate of radiative recombination, which depends on the number of carriers still in the excited state. The experiment thereby gives information about the rate at which the charge carriers leave the excited state, whether by radiative or non-radiative recombination or by transfer to other energy states or to other parts of the structure.

The rate R at which the charge carriers recombine radiatively across the band gap depends on the amount of available electrons and holes and a recombination rate that measures how efficiently the charge carriers recombine.

$$R = Bnp \tag{2.1}$$

B is the so called bimolecular recombination coefficient. The total amount of electrons and holes, n and p in the equation above, is the sum of the number of charge carriers in the structure at equilibrium, n_0 and p_0, and the number of charge carriers created by the optical excitation, Δn and Δp. Using that

$\Delta n = \Delta p$, since the holes and electrons are generated and recombine in pairs,

$$R = B(\Delta n + n_0)(\Delta p + p_0) = Bn_0p_0 + B(\Delta n)^2 + B\Delta n(n_0 + p_0) \quad (2.2)$$

The first term on the right hand side is the equilibrium rate of recombination. The change in carrier concentration is the difference between the generation rate G and the recombination rate R

$$\frac{dn}{dt} = \frac{dp}{dt} = G - R = G_{excess} - B((\Delta n)^2 + \Delta n(n_0 + p_0)) - R_{other} \quad (2.3)$$

$$\frac{d\Delta n}{dt} = G_{excess} - B((\Delta n)^2 + \Delta n(n_0 + p_0)) - R_{other} \quad (2.4)$$

In the last equality of (2.3) it is used that the equilibrium recombination rate is equal to the equilibrium generation rate. The generation rate of excess carriers G_{excess} includes generation from optical excitation, but can also include transfer of charge carriers from nearby regions in a heterostructure, for example the transfer of carriers from the large band gap shell to the core in a core-shell nanowire. R_{other} includes all other recombination processes but the radiative recombination across the band gap, primarily non-radiative recombination. The PL intensity is proportional to the rate of radiative recombination and the rate equation (2.4) can be used to model the PL decay. Chapter 4 describes how such modelling can be used for core-shell nanowires in order to investigate the transport of charge carriers from the shell to the core.

If we now switch off the optical excitation, $G_{excess} = 0$ and the number of excess charge carriers decay only by radiative recombination. Two simple cases can then be distinguished, depending on the level of optical excitation. In the first case there is a low level of optical excitation, such that the number of optically generated charge carriers are few compared to the equilibrium concentrations n_0 and p_0,

$$\begin{aligned} \Delta n &\ll n_0 + p_0 \\ \frac{d\Delta n}{dt} &= -B(n_0 + p_0)\Delta n \end{aligned} \quad (2.5)$$

$$n(t) = \Delta n_0\, e^{-B(n_0+p_0)t} = \Delta n_0\, e^{-t/\tau} \quad (2.6)$$

where Δn_0 is the initial excess concentration of charge carriers. The number of carriers decay exponentially with a time constant τ that depends on n_0 and p_0.

The only recombination process considered in (2.5) is the recombination across the band gap. If there are other recombination possibilities, for example non-radiative recombination via the surface or defects in the bulk, those can be included in Equation 2.5 so that

$$\frac{d\Delta n}{dt} = -k_r \Delta n - k_{nr} \Delta n \tag{2.7}$$

where k_r and k_{nr} is the radiative and non-radiative recombination rate, respectively. The effective recombination rate of the charge carriers is the sum of the radiative recombination rate k_r and the non-radiative recombination rate k_{nr}. The non-radiative recombination thus leads to an effective shortening of the carrier lifetime and thereby of the observed PL decay time, which is reasonable since it is an additional channel of recombination. For undoped samples, where the equilibrium charge carrier concentrations are small, the rate of radiative recombination is small (Equation 2.5, $B = 10^{-11} - 10^{-9}$ cm^3/s for III-V materials with direct band gap [18]). Therefore, unless the crystal is of high quality and the surface is well passivated, the non-radiative recombination dominates, and controls the PL decay time [19].

If the number of optically generated charge carriers are *not* few compared to the equilibrium concentrations n_0 and p_0, because of high optical excitation power, the recombination across the band gap can be described with the following equations

$$\begin{aligned} \Delta n &\gg n_0 + p_0 \\ \frac{\Delta n}{dt} &= -B(\Delta n)^2 \end{aligned} \tag{2.8}$$

$$n(t) = \frac{1}{Bt + \Delta n_0^{-1}} \tag{2.9}$$

As time passes and the charge carrier density decreases by recombination, low-level excitation conditions will be reached, and this non-exponential decay will go over to the exponential decay of Equation 2.6, as illustrated in Figure 2.2.

In nanowires the equilibrium concentrations of free carriers can be quite low, since the Fermi level pinning at the surface states results in a band bending and a depletion region extending throughout the nanowire (for low doped nanowires), as discussed in Chapter 3. The situation is then comparable to that for the undoped samples discussed above. The recombination at the surface is further discussed in Chapter 3.

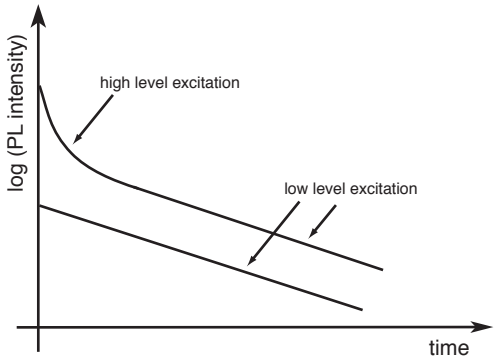

Figure 2.2: The decay of the PL intensity when the initial excitation corresponds to high level and low level excitation, respectively.

2.1.2 Measurement setup

The setup used for the PL measurement in Papers I, II, and V– VII is shown in Figure 2.3. The sample was placed in a liquid He cold-finger cryostat that is equipped with a window and mounted on a translation stage. Laser light was used to excite the sample and it was either focused with a lens, and sent to the sample at an angle, giving a spot size of 10-100 μm or sent through and focused by the microscope objective for more local excitation or higher excitation power density. The luminescence signal was collected by the microscope objective, filtered to remove the scattered laser light, and passed to a spectrometer. The light was detected with a liquid nitrogen cooled CCD (charge coupled device) camera. The spectrometer and CCD camera was also used to image the sample, by using the grating as a mirror (in the zeroth order), to locate the nanowire or the polymer to be studied. For the time-resolved PL measurements a pulsed laser was used for excitation and a streak camera was used as a detector, giving a both spectrally resolved and time-resolved image. For the PL decays from the core-shell nanowires shown here, the signal was summed over all wavelengths emitted by the shell and the core respectively.

2.2 Photocurrent spectroscopy

The PL energy carries information primarily about the lowest excited state(s). Another approach to studying properties of a material is to study the light absorption, which, in contrast to PL, probes higher excited states as well.

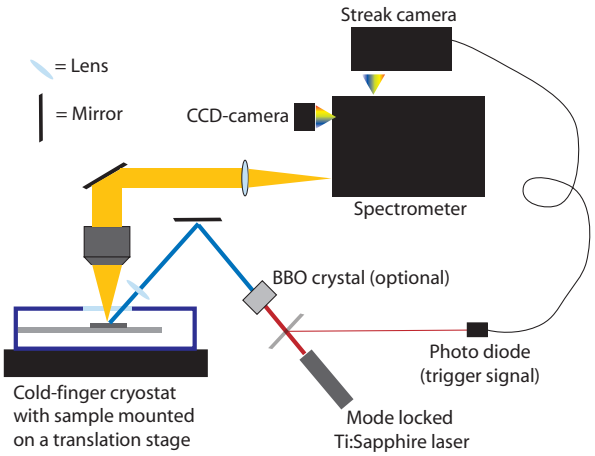

Figure 2.3: The setup for the PL measurements. The mode-locked laser and the streak camera are used for the time-resolved PL measurements. The microscope that was used to collect the luminescence is represented by its microscope objective.

For a semiconductor this means that with absorption spectroscopy the band structure can be studied, whereas PL measurements primarily give information about the band gap and energy levels in the band gap.

The absorption coefficient α is proportional to the joint density of states in the semiconductor, i.e. the number of state "pairs" that can absorb the light at a specific energy. The absorption is thus a picture of the band structure, with some optical selection rules added, since only the optically allowed transitions can be observed. For direct band gap bulk material the joint density of states depends on the photon energy E as

$$\alpha \propto \sqrt{E - E_g} \tag{2.10}$$

where E_g is the semiconductor band gap. Thereby, for photon energies below the band gap, there is no absorption and thus the onset of the measured absorption is a measurement of the band gap.

The most obvious way to measure the absorption is to pass light through the sample under study, and detect the intensity of the transmitted light with a photodetector as a function of its wavelength. This method demands that the absorption in the material is substantial, since it is difficult to detect very small changes in a large light intensity. Another possibility to measure the absorption is to do photocurrent measurements. In this method a bias voltage is applied to the sample, creating an electric field in the material that separates the optically excited electrons and the holes. The increase in number of free carriers gives rise to an increased current. Thus the sample acts

as a photodetector for the light, and the magnitude of the current is related to the amount of absorbed light, and it is thus a measure of the absorption. This method gives information about the transport from the excited state through the material and about the absorption. The transport information can, however, not really be separated from the absorption information. In addition, the structure under study has to be conductive in its excited state.

A single nanowire would correspond to a too small absorption in a transmission measurement, and that is therefore not a suitable method for single nanowire spectroscopy. In a photocurrent measurement, however, only the light that is absorbed and that generates free carriers in the nanowire is detected. As long as the excitation intensity is high enough to generate a substantial current, the absorption in the single nanowire can be measured by contacting only one nanowire at a time. Even if a large area of the sample is excited, as in this work where the excitation spot size is about 1 cm, absorption in other, not contacted parts of the sample is not detected. The background in the photocurrent measurement is the dark current in the nanowire.

The drawback of photocurrent spectroscopy is that it requires reasonably good contacts to the nanowire. The nanowires studied with photocurrent spectroscopy in this thesis are InAs nanowires with a centrally placed $InAs_{1-x}P_x$ segment, and the contacts are made to the InAs ends of the nanowire. It has been shown that contacts to InAs nanowires are ohmic at temperatures above 200 mK [20]. In addition, the band edge offset between the InAs and the $InAs_{1-x}P_x$ reduces the dark current. This choice of structure thus enables low background photocurrent spectroscopy (of the $InAs_{1-x}P_x$ segment) on single nanowires.

2.2.1 Measurement setup

The photocurrent measurements were performed using a Fourier transform spectrometer. A bias voltage in the range from a few tens of mV up to a few V was applied to the sample. Typical all-wavelength photocurrents were in the 0.1-1nA range. The large spread in the necessary voltage to get a sufficient photocurrent might indicate that the contacting was not always successful, so that the contact were non-ohmic. This is not critical for measuring the onset of the photocurrent, but the IV-curves should be interpreted with some caution. The measurements were performed at a temperature of 5 K. For that purpose, the sample was mounted in a He cryostat equipped with a window, where the sample is in cold He gas, in contrast to the cold-finger cryostats used for the PL-measurements.

2.3 Nanowire growth and sample preparation

2.3.1 Nanowire growth

The III-V nanowires studied in this thesis were grown by epitaxy from a semiconductor substrate. The two epitaxy methods used for the nanowire growth are chemical beam epitaxy (CBE) and metal-organic vapor phase epitaxy (MOVPE). A detailed description of the epitaxy is outside the scope of this thesis, and this section only briefly describes the growth. Descriptions of nanowire growth and growth mechanisms can be found in [2, 21] for CBE and [22–24],[Paper II] for MOVPE.

The nanowire growth is seeded by Au aerosol particles. The Au particles are deposited on a (111)B substrate. The particles locally enhance the growth rate, by collecting the group III material, leading to a supersaturation of the particle and thereby a driving force for crystallization of material under the particle. The nanowire thus grows underneath the particle at the Au-nanowire interface and the diameter of the nanowire is controlled by the Au particle size. The nanowires grow perpendicular to the surface of the substrate. With the appropriate growth conditions, the growth on the side facets of the nanowire and the substrate surface is much slower than the growth underneath the Au particle. The growth conditions can be changed by changing the temperature, making growth on the side facets of the nanowire more favourable. This is used to grow a shell of a different material around the nanowire, creating a radial heterostructure. There is, however, still a substantial growth rate under the Au particle [25],[Paper II]. The structure will thus be capped also on the top, but due to difference in growth conditions under the particle and on the side facets of the nanowire, ternary materials may have different composition in the material grown under the Au particle and in the shell. A scanning electron microscope (SEM) image of core-shell nanowires is shown in Figure 2.4.

2.3.2 Sample preparation

For the PL measurement on single nanowires, the nanowires were removed and transferred from the substrate on which they were grown, by touching the substrate with a small piece of clean-room tissue. The wires were then deposited on a patterned substrate by sweeping the tissue across the surface. The pattern allows individual nanowires to be located and studied. It is also possible to study the nanowires still standing on the substrate on which they are grown. If the substrate is a different material than the nanowire, the nanowire signal can be separated from the PL from the substrate. If

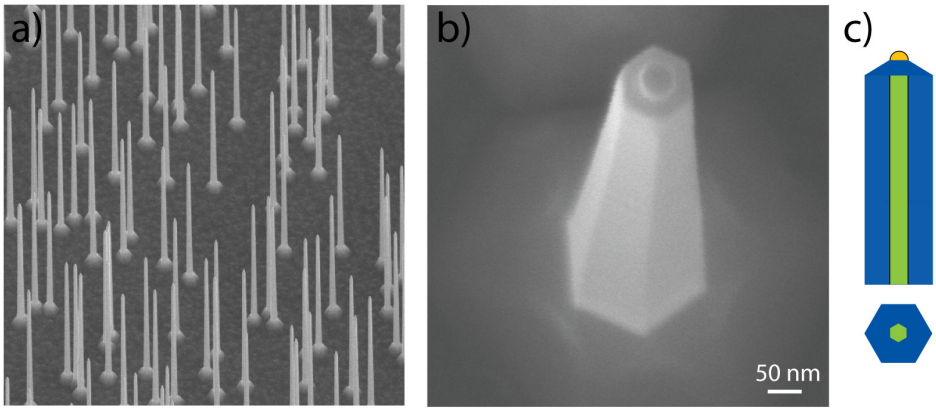

Figure 2.4: SEM images of GaAs/AlGaAs core-shell nanowires on a GaAs (111)B substrate. In a) the sample is tilted 30°. The nanowires are about 8 μm long. In b) the sample is viewed close to perpendicular to the substrate. The round feature seen on top of the nanowire in b) is the Au particle. c) A schematic of a core-shell structure.

the nanowires are grown sparsely enough on the substrate, they can also be studied as individual nanowires in this configuration.

Photocurrent measurements were done on InAs nanowires with a 1 μm long, centrally placed, $InAs_{1-x}P_x$ segment. The crystal structure of the nanowires was characterized using high resolution transmission electron microscopy (HRTEM), and the composition was determined by X-ray energy dispersive spectroscopy (XEDS) in TEM.

In order to contact single nanowires, the nanowires were broken off and picked up from the substrate where they were grown, in the same way as for the PL measurements. The nanowires were then deposited on an n-type Si substrate with a 100 nm thick SiO_2 layer. Prior to the nanowire deposition a pattern was made on the SiO_2 surface to facilitate the nanowire contacting: Bond pads were made by evaporating Ti and Au on the substrate with a TEM-grid as a mask and a coordinate system was defined in the gaps between the bond pads by electron beam lithography (EBL) and subsequent metal (again Ti and Au) evaporation and lift-off. The nanowires were then located on the coordinate system with an SEM . Thereafter, contacts to the InAs ends of the nanowires were defined with EBL. The nanowire contacts were then treated with NH_4S_x to remove surface oxide and passivate the nanowire surface. Finally, Ni and Au was evaporated to make the contacts. This is a contacting scheme that has been previously developed by and described in Reference [26], and it has been shown that contacts to InAs nanowires

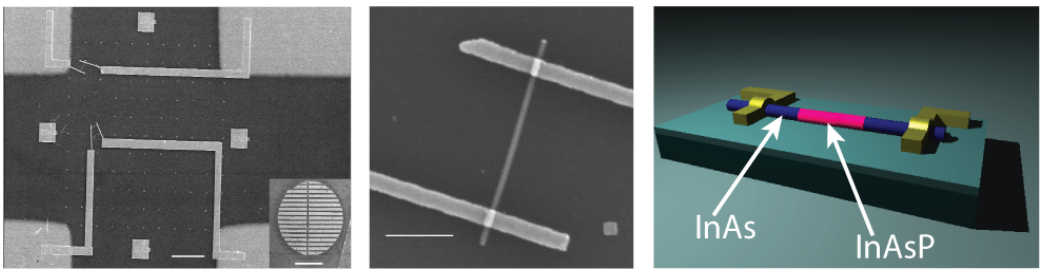

Figure 2.5: Left: SEM image of the EBL-defined coordinate system in the gap between the bond pads, and the contacts to the nanowires, scale bar is 10 μm. The inset shows the bond pads, scale bar is 1 mm. Middle: The contacted nanowire. Scale bar is 1μm. Right: Schematic drawing of the contacted nanowire. Note that the contacts are made to the InAs ends of the nanowire. The schematic drawing was made by Carina Fasth.

fabricated in this way are ohmic at temperatures above 200 mK [20]. The patterned substrate and the contacted nanowire can be seen in Figure 2.5.

For the samples used in Paper VII, the contacting scheme was similar with EBL defined contacts to the nanowire ends, as described in Ref. [27].

The sample preparation for the PL measurements on single MEH-PPV chains is described in Chapter 6.

Chapter 3

Surface states and band bending in nanowires

The surface of the semiconductor crystal corresponds to a large disruption in the periodicity of the crystal. Since the band structure and the band gap of the semiconductor is related to the periodicity of the crystal, the electronic states at the surface will be modified. The electronic structure is also modified by atoms adsorbed at the surface, for example oxygen, and the result is often energy levels in the band gap. These surface states pin the Fermi level of the material at a specific energy at the surface [28]. The situation for a p-type bulk material with surface states in the middle of the band gap is illustrated in Figure 3.1; Far away from the surface, the Fermi level has the same position relative to the band edges as dictated by the doping. The material is depleted of free carriers over a distance w_{bulk}, that depends on the doping of the material, and with higher doping, w_{bulk} is smaller. The shape of the bands can be obtained by solving the Poisson equation,

$$\Delta\Psi = -\frac{\rho}{\varepsilon} \tag{3.1}$$

where ρ is the space charge per unit volume, Ψ is the potential and ε is the dielectric constant of the material. For a region depleted of free charges the space charge is from the ionized dopants.

For a nanowire with a small diameter and a not too high doping level, the depletion region extends throughout the nanowire [29, 30] and the Fermi level in the center of the nanowire is situated far away from both band edges, see Figure 3.1.

The band bending due to the surface states has a number of effects on PL measurements on nanowires. The band banding causes the electrons and

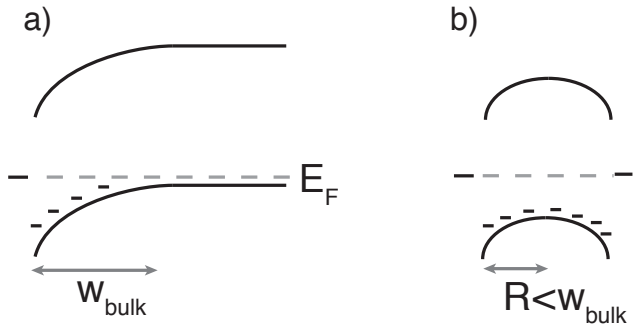

Figure 3.1: a) The surface states, here positioned in the middle of the band gap, pin the Fermi level and induce a band bending. The material is depleted of free carriers up to a distance w_{bulk} from the surface. b) In a nanowire with a radius less than the depletion width in bulk, the material is depleted throughout the entire nanowire.

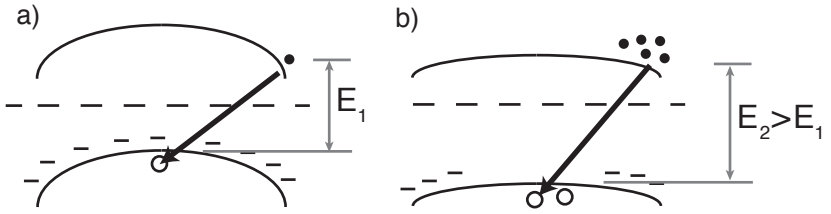

Figure 3.2: a) The band bending causes a spatial separation of electrons and holes, and the PL energy E_1 is less than the band gap. b) At higher excitation power, the electrons and holes form a space charge and thereby flatten the bands. The PL energy then increases to E_2.

holes to be spatially separated, Figure 3.2. Therefore the radiative recombination is slow and the emitted photons have an energy lower than the band gap. As the excitation power is increased, more electrons and holes are excited. These charge carriers form a substantial space charge, neutralizing the donors or acceptors, which leads to flatter bands. The radiative recombination is then more efficient and the PL energy is larger. The PL energy will accordingly increase with increasing excitation power, starting at an energy below the band gap. This has been observed by van Weert et al. for p-doped InP nanowires [31], and in Paper VII this is studied for both p and n-doped InP nanowires.

Since the non-radiative recombination via the surface states requires both electrons and holes, the surface recombination rate is reduced if one type of charge carriers are located some distance away from the surface due to

the band bending [32, 33]. As the bands are flattened by a large number of optically excited charge carriers, both types of charge carriers can reach the surface and the surface recombination is again active. Thus the surface recombination rate depends on the number of excess charge carriers, and thereby on the excitation level [33]. This leads to an initial non-exponential decay of the PL.

The band bending implies that for a moderately doped nanowire, there might not be any free carriers, and then the radiative recombination rate depends on the product of the concentration of the optically generated holes and electrons, as described in Chapter 2 and the PL decay will be non-exponential. This situation prevails also for fairly low concentrations of optically generated charge carriers. However, as the number of excess carriers have decayed enough, the non-radiative recombination processes (other than the surface recombination) will dominate, and determine the PL decay rate.

There are thus two reasons for observing a non-exponential PL decay for short times, and the analysis of the surface recombination used for bulk double heterostructures in for example [33], where the dependence of the surface recombination velocity on the excess charge carrier density is included, might not be sufficient, even if it is adapted to the nanowire geometry. This should be kept in mind when interpreting the PL decay from a nanowire.

3.1 Band bending in *p*- and *n*-doped InP nanowires

For (bulk) InP the surface states are located approximately 100 meV below the conduction band, and the Fermi level is pinned at this position at the surface [28]. This implies that the band bending will be particularly large for a *p*-type InP nanowire.

The shift in the PL energy with excitation power due to the band bending was investigated for *p*-type and *n*-type InP nanowires by PL spectroscopy in combination with an applied gate voltage, and the results are presented in Paper VII. The *n*-type nanowires had a doping concentration of about 6×10^{17} cm^{-3}, estimated from electrical measurements [27]. The doping of the *p*-type nanowires was not know, as it was not possible to extract that from the electrical measurements, due to the highly non-ohmic contacts for those nanowires.

The results from the PL measurements are shown in Figure 3.3. The PL energy was smaller than the band gap for low excitation intensity and shifted to higher energies with increasing excitation intensity, as expected from the

discussion above. The n-doped InP nanowires were mostly of wurtzite crystal structure, where the band gap is about 100 meV larger than the zinc blende band gap of 1.42 eV [34, 35], [Paper IV]. Thus, the PL energies of up to 1.45 eV that were observed here, are still smaller than the band gap. (The p-type nanowires were, however, mostly zinc blende.)

There was also a shift in the PL-peak position with an applied gate voltage. The PL peak positions, extracted by fitting a gaussian to the spectrum, are plotted versus the gate voltage in Figure 3.3. For the p-type nanowires, a positive gate voltage shifted the PL peak to lower energies and a negative gate voltage shifted the PL peak to higher energies. The n-type nanowires displayed the opposite behavior. The large hysteresis effect in the gate dependence could be due to for example water molecules on the nanowire surface [29]. The observed effect of the gate voltage on the PL can be explained as follows: An applied gate voltage changes the amount of carriers in the nanowire. For the p-type nanowire a positive gate pushes out the holes, and fewer acceptors are neutralized by a hole and the band bending increases. A negative gate voltage attracts the holes, which neutralizes the acceptors and thereby flattens the bands. For the n-type nanowires the electrons attracted by the positive gate will neutralize the donors and flatten the bands. This is in agreement with what was observed in the measurements.

These measurements give information about the doping, i.e. the acceptor or donor concentration in the nanowires. In principal, values for the doping level can be extracted from the position of the PL peak. In these measurements, however, the analysis is complicated by that tapering of the nanowires was fairly large, leading to a varying diameter, and thus varying band bending along the nanowire. Furthermore, the tapering is due to that, in addition to the growth under the Au particle, there is a large amount of material grown on the sides of the nanowire. This occurs by a different growth mechanism than the growth under the Au particle, and it cannot be assumed that the doping level is the same in the material grown under the Au particle and the material grown on the sides of the nanowires. In Paper VII, some estimates of the doping concentration are given.

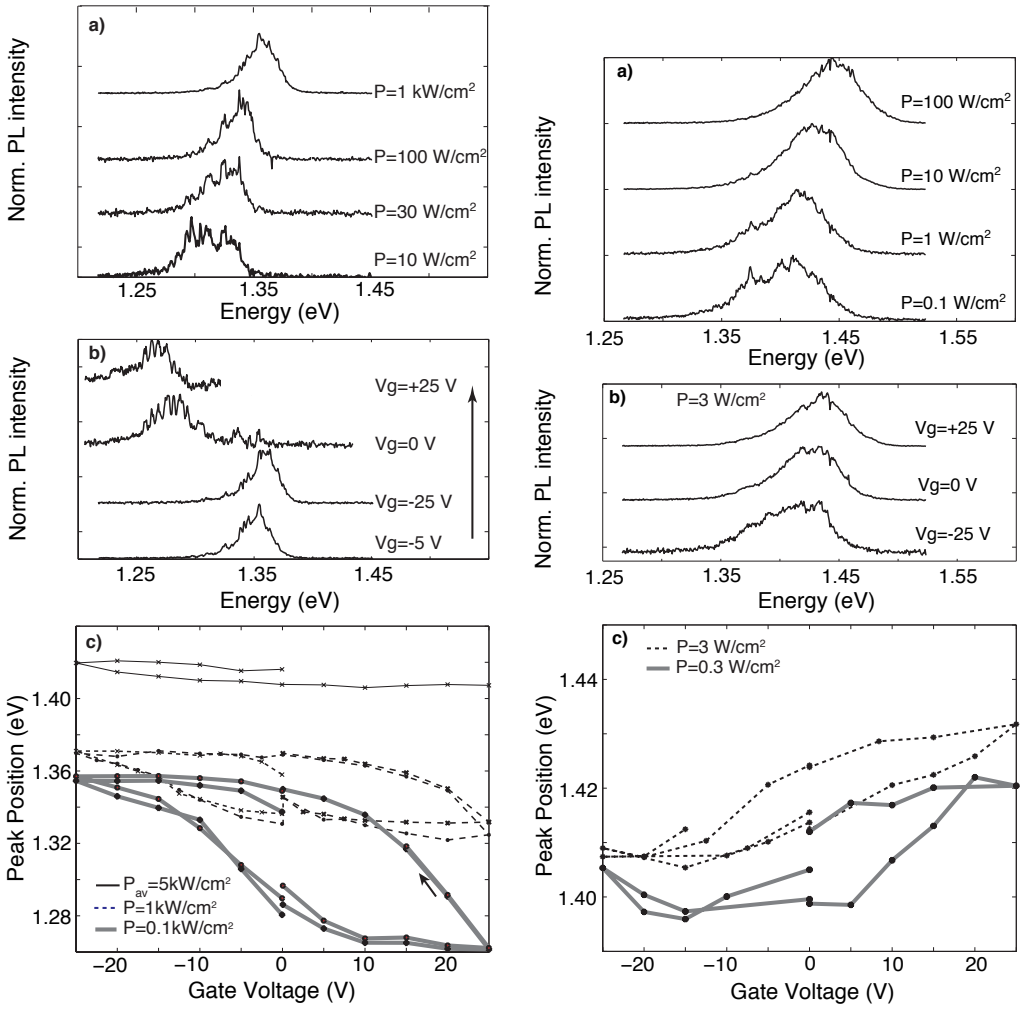

Figure 3.3: Left: PL spectra and the PL-peak position at different gate voltages and excitation intensities for a p-type InP nanowire. The arrows in b) and c) indicate the sweep direction of the gate voltage. Right: PL spectra and the PL-peak position at different gate voltages and excitation intensities for an n-type InP nanowire. The peak-like features in the spectrum are due to etalon effects in the CCD camera chip. The small jump in the hysteresis curve at zero gate voltage is just an artifact of how the gate voltage is applied. The temperature was 10 K.

Chapter 4

Core-shell nanowires

This chapter discusses surface passivation and radial heterostructures in nanowires. The interface quality and the transport of charge carriers from the shell to the core in GaAs/GaInP core-shell nanowires is investigated by time-resolved PL spectroscopy. The effect of strain from a lattice mismatched shell on the PL efficiency of the core is also discussed.

4.1 Surface passivation and radial heterostructures

As discussed in the two previous chapters, the surface states of semiconductor materials act as non-radiative recombination centers, reducing the luminescence efficiency. This is a problem, and particularly so for nanowires where the surface to volume ratio is large. Also, the Fermi level pinning at the surface induce band banding and a region depleted of free carriers, that can extend through a substantial part of the nanowire. Thus, surface passivation is important for optical as well as for electronic applications. The surface passivation can be accomplished by a chemical process, where the dangling bonds at the surface are terminated with for example sulphur atoms [32, 33]. The surface can also be passivated by growing a large band gap shell around the nanowire. Thereby, the crystal lattice is continued and the surface states are separated from the charge carriers confined in the core [10–12], Paper II.

The core-shell layout also introduces an additional degree of freedom in the design of nanowire structures, and devices such as core-shell nanowire LEDs [13, 14] [Paper VI] and nanowire field-effect transistors in a core-shell configuration [15, 16] have been demonstrated. Furthermore, by growing multiple shells, core-shell nanowires can be used to define a radial quantum

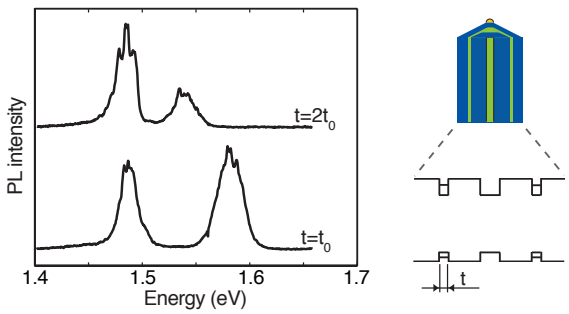

Figure 4.1: PL spectra from two nanowires with a radial GaAs quantum well with AlGaAs barriers. The two nanowires have different thickness of the quantum well. A schematic of the cross-section of the structure is also shown, where light grey corresponds to GaAs and dark grey to AlGaAs. From the position of the PL peak it can be estimated the thickness of the quantum well is 12-15 nm and about 5 nm respectively. The PL peak with energy slightly below 1.5 eV is from recombination via carbon acceptors in the GaAs core.

well [36, 37]. PL spectra from such quantum wells in GaAs/AlGaAs core-shell nanowires are shown in Figure 4.1

By using a shell with larger band gap than that of the core, the core-shell structure allows the combination of carrier confinement in the core and photon confining in the whole nanowire. The shell is then used to design an optimal cavity or a waveguide while the core is kept narrow to confine the charge carriers [38]. The core can even be chosen narrow enough to allow for quantum confinement.

Finally, applying a lattice mismatched shell introduces pseudomorphic strain in the core, adding strain to the methods for band structure engineering [39], [Paper II].

4.2 GaAs/$Ga_xIn_{1-x}P$ core-shell nanowires

4.2.1 Time-resolved photoluminescence spectroscopy

In Paper II results from PL measurements on GaAs nanowires with $Ga_xIn_{1-x}P$ shell are presented. The interface quality and the charge carrier transport from the shell to the core was studied using time-resolved PL spectroscopy on single nanowires. A PL decay for such a nanowire is shown in Figure 4.2.

The decay of the PL from the core was fast, with a decay constant of about 100 ps. This is comparable to the <80 ps reported by [12] for GaAs/AlGaAs core-shell nanowires. The decay was exponential with a initial flatter part

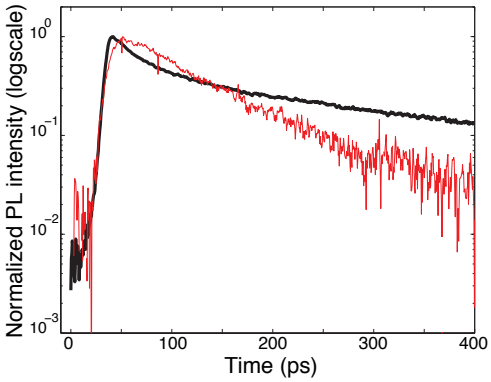

Figure 4.2: The decay of the PL from the core (thin line) and the shell (thick line) of a 40 nm GaAs nanowire with an 80 nm close to lattice matched GaInP shell. The temperature is 10 K.

during the first approximately 10 ps. There were, however, also nanowires exhibiting a PL decay without such a plateau. The fast decay of the PL indicates that non-radiative recombination was the dominating recombination process. This is due to either recombination via interface states between the core and the shell or non-radiative recombination in the interior of the core. Although the GaInP shell clearly passivated the surface, as seen by the orders of magnitude larger PL intensity observed for nanowires with a shell, as compared to nanowires without a shell, there could still be other types of interface states formed at the core-shell interface. It was unfortunately not possible to compare the rate of non-radiative recombination for the core-shell nanowires to that of uncapped GaAs nanowires, since GaAs nanowires without shell were too poorly luminescing to be detected one by one with our streak camera. However, previous time-resolved PL studies of GaAs nanowires showed a decrease in the surface recombination rate after surface passivation treatment [32]. The fast PL decay could also be caused by non-radiative recombination via electronic states related to the high twin density in the nanowire. Joyce et al [40], have shown that GaAs nanowires grown under conditions such that the crystal is pure zinc blende display brighter PL than nanowires containing twin defects.

The PL decay from the shell was not exponential, and, more importantly, it was slower than the decay for the core. This indicates that the transport of charge carriers from the shell to the core was hindered for a fraction of the charge carriers. If all charge carriers in the shell were free to transfer to the core, the decay would necessarily be at least as fast as the PL decay for the core. For the nanowires where the PL decay exhibited a plateau in the

beginning of the decay, however, some of the charge carriers in the shell must be free to transfer into the core, since a plateau indicates that charge carriers are added to the core at the same rate as that at which they recombine, which can only be explained by charge carriers transferring from the shell.

The PL decay can be modelled using the rate equations in Chapter 2. The recombination in core as well as the recombination in the shell was modelled by a single recombination rate, including both radiative and non-radiative recombination, and only terms linear in n were considered. For the core, this is justified since the PL decay appeared exponential. For the shell, however, it could be an oversimplification, as discussed below. The rate equations are given below, and the transfer and recombination possibilities are illustrated in Figure 4.3.

$$\begin{aligned}
\frac{dn_c(t)}{dt} &= -n_c k_c + n_{sc} k_{sc} \\
\frac{dn_{sc}(t)}{dt} &= -n_{sc} k_s - n_{sc} k_{sc} \\
\frac{dn_s(t)}{dt} &= -n_s k_s - n_{sc} k_{sc}
\end{aligned}$$

$$\begin{aligned}
n_c &= n_{sc_0}\beta \exp(-(k_s + k_{sc})\, t) + (n_{c_0} - n_{sc_0}\beta) \exp(-k_c t) \\
\beta &= k_{sc}/(k_c - k_s - k_{sc}) \\
n_s &= (n_{s_0} - n_{sc_0}) \exp(-k_s t) + n_{sc_0} \exp(-(k_s + k_{sc})\, t)
\end{aligned} \tag{4.1}$$

where $n_c(t)$ and $n_s(t)$ are the number of carriers and k_c and k_s are the recombination rates in the core and shell, respectively. In this model only n_{sc} of the carriers in the shell can transfer to the core, and this occurs at a rate k_{sc}. n_{c_0} and n_{s_0} are the initial populations in the core and shell, respectively.

The width of the laser pulse, and thus the duration of the optical excitation, was smaller than the time resolution of the measurement system. Therefore, in the model the initial state is that all carriers are excited, and there is no optical generation included. To compare the model to the data, the model PL decay was convoluted with a Gaussian pulse with a width equal to the time resolution of the measurement system. The decays simulated with this model were compared to the data by varying the parameters, in order to find a set of parameters that reproduced the shape of the decay. The simulated decays are shown in Figure 4.4. The shape of the PL decay with a plateau in the beginning of the decay could be reproduced only if the number of charge carriers free to transfer from the shell to the core was set to about the same size as the number of charge carriers optically excited in

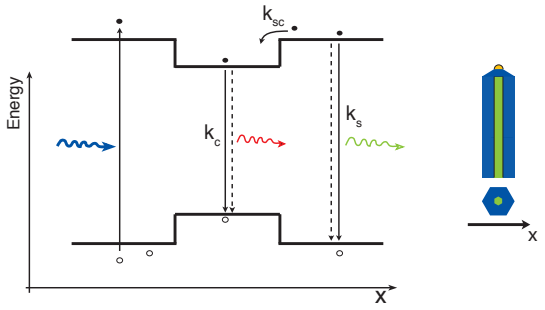

Figure 4.3: A schematic picture of the core-shell nanowire, the band structure of the nanowire and the possible decay processes for the optically excited charge carriers. The solid and dashed lines indicate radiative and non-radiative recombination, respectively.

the core. The model thus supports the interpretation that this behavior is due to transfer of charge carriers from the shell to the core.

To reproduce the shape of the PL decay for the shell with this simple model, the number of charge carriers being able to transfer into the core had to be set to about half the initial population of the shell, which then becomes comparable to the initial population of the core. This might not be reasonable, considering that the volume of the shell was close to 20 times the volume of the core, which implies that the number of optically excited charge carriers in the shell is much larger than in the core (if the absorption coefficient is comparable for the shell and the core). Other reasons for observing a non-exponential decay could be either a charge carrier concentration dependent surface recombination rate, most probably at the outer surface of the shell, or that the optical excitation was enough to produce a high level excitation condition, as discussed in Chapter 3.

To further investigate the charge carrier transfer, the PL decay for the core with excitation energy larger than the band gap of the shell was compared to the PL decay with excitation energy smaller than the band gap of the shell. The data is shown in Figure 4.5. As expected, for the nanowires displaying the plateau in the PL decay, this feature disappeared when selectively exciting the core, confirming that it was due to charge carriers transported from the shell to the core.

For nanowires without this plateau, the only effect of the change in excitation energy was a small reduction of the PL decay time, possibly due to a somewhat different excitation power density, since we observed that (for a fixed excitation energy) an increased excitation power density decreased the PL decay time (data not shown).

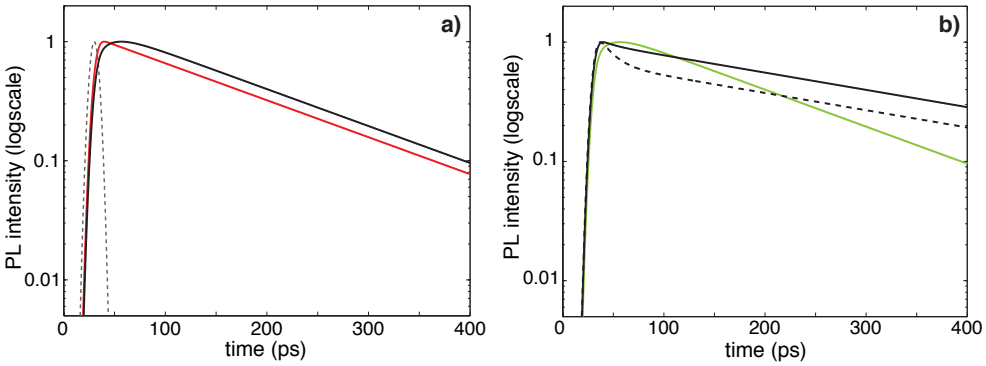

Figure 4.4: a) The modelled PL decay for the core with (black line) and without (red line) transfer of carriers from the shell. The dashed line is the gaussian pulse used to represent the time-resolution of the measurement system. The following parameters were used as input to Equation 4.1: $k_{sc} = 1/15$ ps^{-1} $k_c = 1/140$ ps^{-1} $k_s = 1/300$ ps^{-1}. To model a transfer from the shell $n_{sc_0} = n_{c_0}$, and to model the situation with no transfer $n_{sc_0} = 0$. b) Comparison of the modelled PL decay for the shell with a large fraction of the charge carriers being able to transfer into the core (black dashed line) and small fraction of the charge carriers being able to transfer (black solid line). The modelled PL decay from the core is represented by a green solid line. The parameters used were $n_{s_0} = 2n_{sc_0}$ and $n_{s_0} = 10n_{sc_0}$ respectively. Transfer and decay rates as in a).

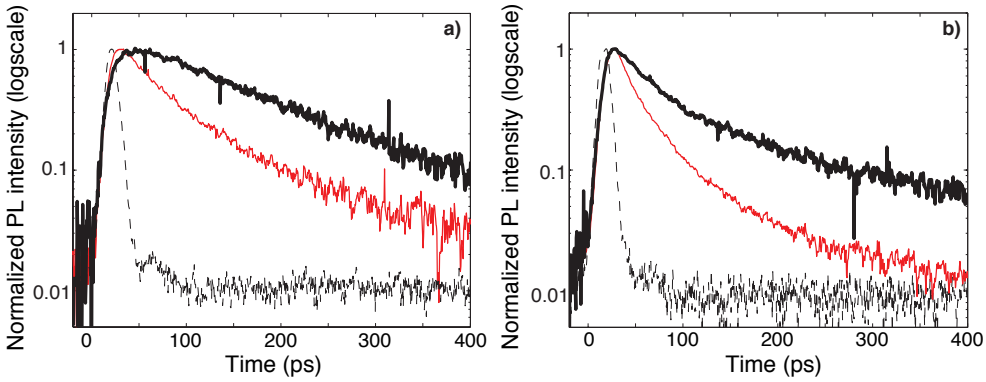

Figure 4.5: The PL decay from the core of two different 40 nm GaAs nanowires with 80 nm GaInP shell. The thick black (thin red) solid line is for excitation energy above (below) the band gap of the shell. The dashed line is the laser pulse. a) PL decay from a nanowire that displayed signs of charge carrier transfer from shell to core. b) PL decay from a nanowire that showed no signs of charge carrier transfer.

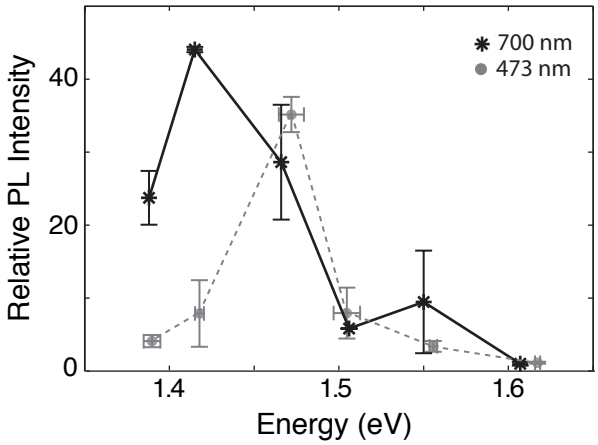

Figure 4.6: PL peak position vs PL intensity from samples with different compositions of the $Ga_xIn_{1-x}P$ shell. The nanowires were grown from GaP substrates, and the PL signal was collected from a large number of nanowires standing on the substrate. The black stars connected with a solid line are measurements with selective excitation of the nanowire core, and the gray dots connected with a dashed line are measurements with an excitation energy such that both core and shell is excited. The errorbars show the variation at different points on the sample. Room temperature measurements.

4.2.2 Effects of strain on the PL intensity

Paper VI presents results that showed that the composition of the shell affected the intensity of the PL from the nanowire core in GaAs/$Ga_xIn_{1-x}P$ core-shell nanowires. In Figure 4.6 the PL intensity for nanowires with different compositions of the shell is shown both for excitation with an energy smaller than and larger than the band gap of the shell. For the data obtained when selectively exciting the core, it was found that the maximum PL intensity is obtained for unstrained samples. The PL intensity measured with an excitation energy larger than the band gap of the shell is affected by the absorption in the shell and the transport of charge carriers from shell to core. This could explain that the maximum PL intensity was obtained for different shell compositions depending on the excitation energy.

One explanation for the decrease in PL intensity with increasing strain, could be that there is a mismatch between the emission polarization direction that is induced by the strain, and the polarization direction required for wave-guiding the light through the nanowire. The argument is as follows: For planar layers, biaxial strain splits the degeneracy of the valence band at $k = 0$. Under compressive strain, the heavy hole band is the low energy

state for the holes, and most of the radiative recombination therefore takes place between the heavy hole band and the conduction band, and vice versa for tensile strain. Due to the difference in the symmetry of the two bands, the polarization of the emission from the heavy hole band is parallel to the plane of the layer, whereas the emission from the light hole band is partially polarized perpendicular to the layer [41]. It is non-trivial to extend this to the situation in the strained nanowire core. However, similar effects should exist, and thereby, the polarization of the emission possibly depends on the strain.

The emission from an unstrained nanowire can be polarized for at least two reasons; For a nanowire with a diameter that is small compared to the wavelength of the light, the difference in dielectric constant of the nanowire and its surrounding causes the emitted light to be polarized along the nanowire axis [42]. (This is further discussed in Chapter 5). For a nanowire with a large diameter the light can be wave-guided by the nanowire [43],[Paper II], and the different modes of the waveguide correspond to different polarizations of the guided light.

In this experiment the diameter of the nanowire was 140 nm, and the light was (at least partially) wave-guided out through the ends of the nanowire. Also, the nanowires were studied standing on the substrate and in this measurement configuration primarily the light emitted from the ends is observed. The observed emission intensity then depends on how strongly the light is coupled to the guided modes [43]. If the nanowire is strained, and the strain affects the polarization of the light, it could also affect the coupling to the waveguide, and thus the observed emission intensity. This could potentially explain that the emission efficiency depends on the strain, at least in one of the strain directions.

In order to fully understand the dependence of the PL intensity on the strain, further investigations are needed, for example PL measurement on nanowires with different diameters to tune the possibility for wave-guiding of the light.

Chapter 5

Nanowire crystal structure and the optical properties

The III-V semiconductors have two possible crystal structures; the cubic structure zinc blende and the hexagonal structure wurtzite. With the exception of the III-nitrides, most III-V semiconductors have a zinc blende crystal structure when in bulk form. For III-V nanowires grown in the [111]B direction (which is the most commonly observed growth direction for III-V nanowires [17, 44]), however, both crystal structures, or an alternation between the two, are observed [2, 17, 34, 35, 40, 45–47]. The zinc blende and the wurtzite crystal structures have different material properties such as band gap [48], and effective masses and also different selection rules for optical transitions [49]. In this Chapter, measurements of the band gap of the alloy $InAs_{1-x}P_x$ with wurtzite crystal structure are presented. Furthermore, the effects of the type II offset between the two crystal phases on the excitation power dependence of the PL from rotationally twinned InP nanowires is presented. These results are further discussed in Papers III, IV and V.

5.1 Crystal structure

The zinc blende and wurtzite crystal structures differ in how the atomic bilayers of group III and group V atoms are stacked, as illustrated in Figure 5.1. The ABCABC stacking sequence is the structure of zinc blende, and the ABABAB stacking sequence is the structure of wurtzite.

Apparently, the two crystal structures are similar, and the difference between the ABC stacking and the ABA stacking is only a 60 degree rotation about the [111]-axis of the last layer. If one of the layers in a zinc blende crystal ends up in position A instead of C, the structure becomes

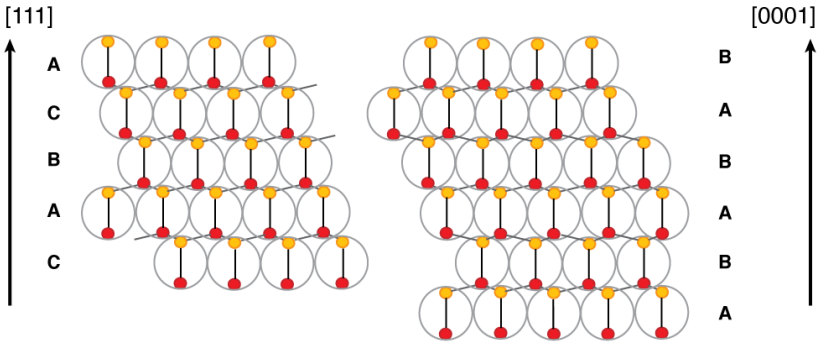

Figure 5.1: The stacking sequence in zinc blende (left) and wurtzite (right) crystals in the [111] direction ([0001] direction for wurtzite). The light and dark filled circles correspond to the two types of atoms in the III-V semiconductor. The larger gray circles are guides to the eye to illustrate the stacking sequence.

ABCABACBACB, where the wrongly stacked layer is marked in gray. This is referred to as rotational twinning. The crystal (the twin) above the twin plane is rotated 180 degrees about the [111] axis relative to the segment (twin) below the twin plane. As can be seen, the interface between the two twins can be interpreted as a very short segment with wurtzite symmetry (ABC*ABA*CBACB).

Such rotational twinning is frequently observed in III-V nanowires grown in the [111]B direction, and the nanowires often have a high density of twin planes [12, 50, 51], [Papers V and II]. The crystal structure for the nanowires grown in the [111] direction depends on the growth conditions [45, 50, 52], and it has been demonstrated that it can be controlled to some extent [35, 40, 50]. Nanowires grown in the [100] direction, however, are observed to be pure zinc blende crystals [53], [Paper V], since, for that growth direction, there is a larger energy barrier for formation of such twin defects [53].

The frequent rotational twinning results in a number of problems; First, the alternation between the two twins leads to a micro-faceted surface of the nanowire [54], which may result in problems with the growth and composition of shell structures (in particular for shells of ternary materials). In addition, the twin planes formed in the core propagate into the shell material [54]. Secondly, the interface between two twins could possibly contain defect states in the band gap acting as non-radiative recombination centers. The observation that pure zinc blende nanowires have brighter luminescence as compared to nanowires with rotational twins [40, 53] could be an indication of this. Finally, because of the different crystal symmetry, the zinc blende and the wurtzite crystal structures have different material parameters such

as the band gap, and an alternating crystal structure due to rotational twinning, results in a non-intentional heterostructure along the nanowire axis [Paper V].

On the other hand, if the stacking sequence can be controlled, and also changed along the length of a nanowire, this could be utilized as an additional design parameter, for example for rotational twinning superlattices [55].

5.2 Wurtzite and zinc blende – the band structure

5.2.1 The band gap for wurtzite $InAs_{1-x}P_x$

Since the crystal structure and symmetry differs between the zinc blende and wurtzite phases of a material, the band gap is expected to differ, and from calculations the wurtzite band gap is expected to be larger than the zinc blende band gap [48, 56, 57]. For bulk III-V materials, it is only the nitrides that exist in both phases, and for GaN, which is the most studied of the nitrides, the wurtzite band gap is 3.5 eV as compared to 3.3 eV for the zinc blende band gap [58]. For nanowires, pure wurtzite crystals have been observed for the $InAs_{1-x}P_x$ material system [2, 17, 34, 35, 59] and the band gap has been measured to be on the order of 100 meV larger than the zinc blende band gap [34, 35], [Paper IV]. There are also some observations of GaAs nanowires in the wurtzite phase, with a measured band gap only slightly larger than the corresponding zinc blende band gap [46, 60].

As described in Paper IV, we have measured the band gap of $InAs_{1-x}P_x$ nanowires having wurtzite crystal structure as a function of the composition for $0.15 < x < 0.48$. The band gap was measured using photocurrent spectroscopy at a temperature of 5 K. In order to form ohmic contacts to the nanowires, InAs nanowires with a centrally placed $InAs_{1-x}P_x$ segment were used, and contacts were fabricated to the InAs ends of the nanowires. An example of a photocurrent spectrum is shown in Figure 5.2. The onset of the photocurrent is determined by a linear extrapolation of the spectrum, and we interpreted the photocurrent onset as the band gap. The large nanowire diameter (85 nm) implies that quantum confinement effects should be negligible (cf. [61, 62]), and thus the measured band gap should be equal to the band gap for bulk. A plot of the photocurrent onset vs the P content in the $InAs_{1-x}P_x$ segment is shown in Figure 5.2.

For the ternary III–V alloys, the dependence of the band gap E_g on the

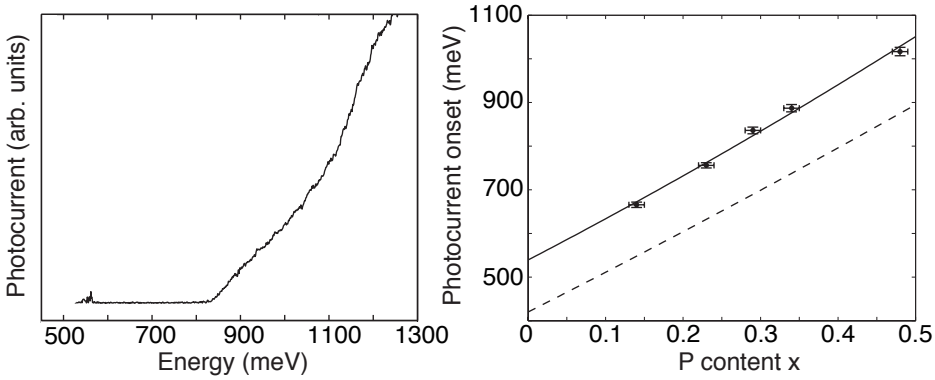

Figure 5.2: A photocurrent spectrum for a nanowire with 29% P in the InAsP segment. Also shown is a plot of the photocurrent onset vs the P content in the $InAs_{1-x}P_x$ segment. The points are the mean current onset values from photocurrent measurements on 6 to 8 nanowires, and the error bars indicate the standard deviation. The solid line is a fit of Eq. (5.1) to the data, using a bowing parameter $C = 0.2$. The dashed line is Eq. (5.1) evaluated with the parameters for zinc blende $InAs_{1-x}P_x$, taken from Ref. [63].

composition can be described with the following relationship:

$$E_g(InAs_{1-x}P_x) = (1-x)E_g(InAs) + xE_g(InP) - x(1-x)C \qquad (5.1)$$

where C is the so-called bowing parameter. The fit of this equation to the data, using a bowing parameter of $C = 0.2$ eV, is shown in Figure 5.2, and for comparison, the band gap for zinc blende $InAs_{1-x}P_x$ calculated from Equation 5.1 using the zinc blende parameters recommended in [63] is also plotted in Figure 5.2. As can be seen, the band gap was approximately 120 meV larger than the band gap for zinc blende $InAs_{1-x}P_x$, over the entire composition range. With $C = 0.2$ eV, the band gaps obtained from the fit are 0.54 eV for wurtzite InAs and 1.65 eV for wurtzite InP (the choice of bowing parameter is discussed in Paper IV).

The observation that the wurtzite band gap was larger than the zinc blende band gap is in agreement with what can be expected, as discussed above. The difference between the obtained band gap for wurtzite InAs and the band gap of zinc blende InAs (0.42 eV at 0 K) is 120 meV and for InP the difference between the obtained wurtzite band gap and the zinc blende band gap (1.42 eV at 0 K) is 230 meV. These increases in band gap can be compared to literature values:

Zanolli et al. [56], calculated the wurtzite InAs band gap to be 50 meV larger than the zinc blende band gap. This is is smaller than, but comparable

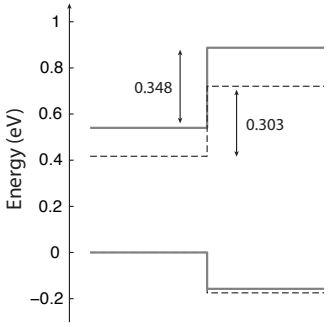

Figure 5.3: An InAs/$InAs_{0.5}P_{0.5}$ heterostructure with zinc blende (dashed line) and wurtzite (solid line) crystal structure respectively. The values for the band gaps are taken from [63] and Paper IV respectively and band offsets from [63] and [2] respectively. The valence band offset is somewhat smaller and the conduction band offset somewhat larger for the wurtzite structure as compared to the zinc blende structure. The valence band edge in zinc blende and wurtzite InAs are both drawn at 0 eV, although there is possibly a type II offset between the two crystal structures [57].

to our measured value. Although InP is outside the measured composition range, it is worth comparing the obtained band gap to literature values. Most published experimental studies, all PL studies, report an increase in band gap of about 80 meV [34, 35, 59]. This is clearly smaller than the 230 meV obtained here, but comparable to the overall 120 meV increase in band gap.

For band gap engineering it is essential to know how the band gap and the band offsets vary with the composition. In [2] the dependence of the conduction band offset on the composition for $InAs_{1-x}P_x$ nanowires with wurtzite crystal structure was investigated. Combining those results with the dependence of the band gap on the composition obtained here, the evolution of both the conduction and valence band offsets with the $InAs_{1-x}P_x$ composition can be determined. An example of the band alignment in an InAs/$InAs_{1-x}P_x$ heterostructure is given i Figure 5.3. As can be seen, there is a difference in band alignment as compared to the zinc blende structure, primarily in the conduction band offset.

5.2.2 The band edge offset between zinc blende and wurtzite InP

As discussed above, rotational twinning is commonly observed in nanowires grown in the [111] direction. The structure of such a nanowire can be described as a zinc blende crystal containing a large number of monolayer-thick wurtzite segments. Calculations predict that the band alignment between the zinc blende and the wurtzite phase in a material is type II for all III-V semiconductors [57], with the valence band edge for the wurtzite material above the valence band edge for the zinc blende material. This has also been shown experimentally for GaN [64]. This can have a significant effect on the optical properties of the nanowires.

In Paper V the effect of this type II offset on the PL for InP nanowires is discussed. The excitation power dependence of the PL spectrum from InP nanowires having a high frequency of rotational twins was compared to that of InP nanowires having a pure zinc blende crystal structure. It was observed that as the excitation intensity increased, there was a large blueshift of the PL spectrum for nanowires with rotational twins, whereas the nanowires free from rotational twins did not display such a shift. This was attributed to that the type II offset causes the electrons to localize in the (zinc blende-like) regions of the nanowire with few rotational twins, and the holes to localize in the (wurtzite-like) regions with a high density of rotational twins, see Figure 5.4.

Adjacent zinc blende-like and wurtzite-like regions act as the two sides of a type II heterostructure (of different materials) as described in [65, 66]. In such structures, the separation of the electrons and holes across the type II interface induces an electric field and band bending, as illustrated in Figure 5.5. For low excitation powers, an increase in optically generated charge carriers concentration increases the band bending, and the PL spectrum blueshifts. As the excitation power is increased further, it is rather a band-filling effect that causes the blueshift of the PL. These shifts are then somewhat larger [65, 66], and a plot of the PL energy vs the excitation power should have two slopes. This was not seen in the measurements presented in Paper V, which may be attributed to the more complex situation for these nanowires with several heterojunctions, and different widths of the zinc blende-like and wurtzite-like regions.

When comparing these results to other PL measurements on nanowires with rotational twins it should be noted that the separation of electrons and holes is critically dependent on the distribution of the twin planes. In the nanowire studied by both TEM and PL in Paper V, there really were

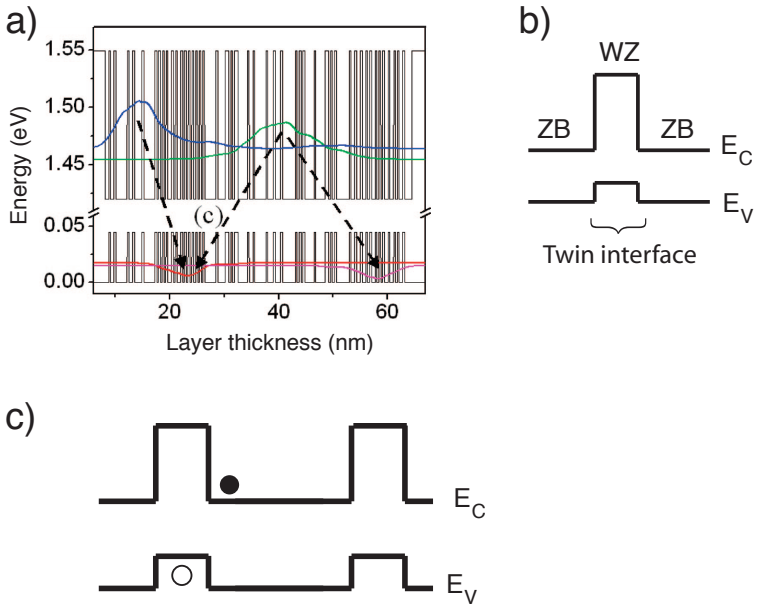

Figure 5.4: a) The probability density for the electrons and holes in a segment of a rotationally twinned InP nanowire. The potential is constructed from a TEM image of the nanowire. Each twin interface is represented by a monolayer of wurtzite InP. The image is taken from Paper V. b) The band structure at the twin interface (ZB=zinc blende, WZ=wurtzite). c) The resulting potential in the rotationally twinned structure in a)

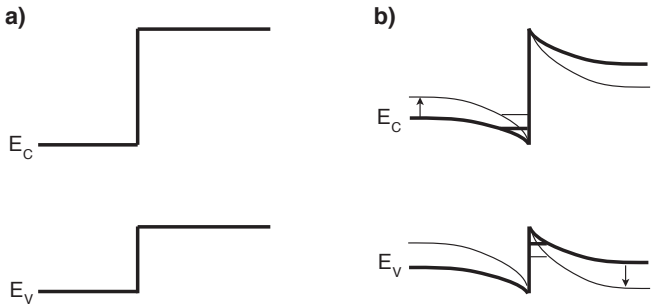

Figure 5.5: a) A type II heterostructure. b) The optically excited electrons and holes create an electric field that induces band bending. The band bending increases with increasing excitation intensity (indicated by the arrows) and shifts the subbands to higher energies.

wurtzite-like regions separated by longer regions with few twin planes, as seen in Figure 5.4. If the twin planes are more evenly distributed there is very little localization, in particular for the electrons. This could partly explain that a number of nanowires in the study presented in Paper V could neither be categorized as rotationally twinned nor as pure zinc blende from their spectral behavior.

However, the results in Paper V support that the offset between zinc blende InP and wurtzite InP is type II, and this result could be relevant both for interpretation of data from optical measurements and for the suggested wurtzite-zinc blende superlattices suggested by [55].

5.3 Polarization effects

For free-standing nanowires, where there is a large difference in dielectric constant of the nanowire and the surrounding medium (air), it has been observed that the PL is strongly polarized along the nanowire axis [12, 35, 67–69], and that the absorption is stronger for light polarized along the nanowire axis [12, 67–69].

In Paper III, InAs nanowires with a centrally placed $InAs_{1-x}P_x$ segment were studied using photocurrent spectroscopy. Photocurrent spectra for excitation light polarized perpendicular and parallel to the nanowire are shown in Figure 5.6.

The polarization dependence of the photocurrent can be explained by assuming that the nanowire responds to the excitation light as an infinitely long dielectric cylinder with a dielectric constant ε_w, surrounded by a medium with dielectric constant ε_0. This is the same model as used in Refs [12, 35, 67–69]. If the incident electric field is oriented perpendicular to the nanowire, i.e. if the excitation light is polarized perpendicular to the nanowire, the electric field inside the nanowire is attenuated compared to the incident electric field. An electric field oriented parallel to the nanowire is not attenuated [70]. The absorption thus depends on the polarization of the excitation light. From this model the degree of polarization σ of the absorption can be calculated:

$$E_{\parallel} = E_0 \tag{5.2}$$

$$E_{\perp} = \frac{2\varepsilon_0}{\varepsilon_0 + \varepsilon_w} E_0 \tag{5.3}$$

$$I \propto E^2 \tag{5.4}$$

$$\sigma = \frac{I_{\parallel} - I_{\perp}}{I_{\parallel} + I_{\perp}} = \frac{(\varepsilon_0 + \varepsilon_w)^2 - 4\varepsilon_0^2}{(\varepsilon_0 + \varepsilon_w)^2 + 4\varepsilon_0^2} \tag{5.5}$$

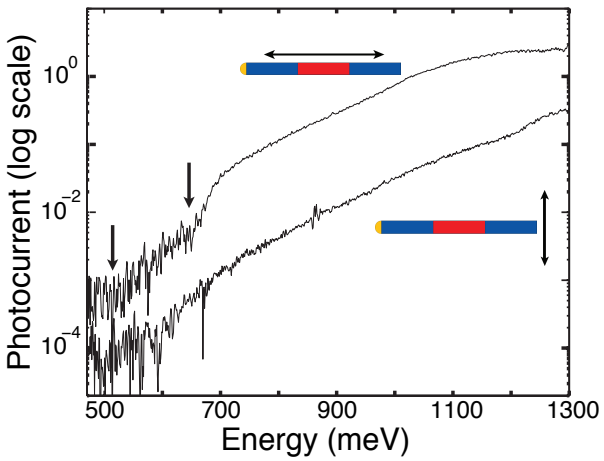

Figure 5.6: Photocurrent spectrum for excitation light polarized parallel and perpendicular to the nanowire axis. The two photocurrent onsets are indicated with arrows. The photocurrent signal with the onset at the lower energy is attributed to excitation in the InAs ends of the nanowire, or the $InAs_{1-x}P_x$ shell non-intentionally grown on the lower InAs segment. The other onset is attributed to excitation in the $InAs_{1-x}P_x$ segment. The P content in the $InAs_{1-x}P_x$ segment is 14%.

where E_0 is the incident electric field and $E_\parallel$ and $E_\perp$ is the electric field inside the nanowire for parallel and perpendicular orientation of the incident field, respectively. $I_\parallel$ and $I_\perp$ are the corresponding absorbed intensities. With the values for the dielectric constant of the nanowire, $\varepsilon_w = 12.4$, which is the dielectric constant for InP, and the dielectric constant $\varepsilon_0 = 1$ for the surrounding air, the degree of polarization of the absorption, and thus of the photocurrent, is $\sigma = 0.96$. The emission will also be polarized due to the difference in dielectric constant between the nanowire and its surroundings, but with a smaller degree of polarization [42].

The measured degree of polarization of the photocurrent added for all excitation wavelengths was in the range from $\sigma = 0.8$ to $\sigma = 0.93$. Thus, the dielectric contrast between the nanowire and its surroundings is enough to account for the observed degree of polarization. For some nanowires, the photocurrent spectra showed a difference in the degree of polarization for different energy ranges, and that could indicate that the obtained values are an underestimation of the degree of polarization of the absorption in the $InAs_{1-x}P_x$ segment, as further discussed in Paper III.

From quantum mechanics we know that the absorption is governed by selection rules for the optical transitions. The model discussed above does

not include such selection rules, or any polarization dependence of these. For a zinc blende crystal optical transitions from the top of the valence band to the conduction band are allowed for both polarizations, and thus the model above fully explains the polarization dependence (for nanowires with diameters large enough that quantum confinement effects are negligible) [68]. For a crystal with wurtzite structure, however, the (different) symmetry of the crystal leads to different selection rules for optical transitions as compared to a crystal with zinc blende structure [35, 49, 71]. The transition from the top valence band to the conduction band is allowed for light polarized perpendicular to the [111] direction, but forbidden for light polarized parallel to the [111] direction, at least at the Γ-point.

For nanowires with wurtzite crystal structure and the c-axis parallel to the growth direction this means that the dielectric contrast makes absorption and and emission of light with polarization along the nanowire axis favourable, but the selection rules only allow emission and absorption with polarization perpendicular to the nanowire axis [49, 71].

The shape of the nanowire, and the wavelength of the excitation or emission determines which effect will dominate, the dielectric contrast or the selection rules [69]. The smaller the aspect ratio of the nanowire, the smaller the effect of the dielectric contrast [70]. Also, nanowires that are fairly tapered should have a smaller polarization dependence due to the dielectric contrast [12]. For the simple model discussed above to be valid, the wavelength of the light has to be much larger than the diameter of the nanowire [42]. If this is not the case, the effect of the difference in dielectric constants will be small or zero. In literature different polarization dependences for nanowires with wurtzite crystal structure has been observed. Shan et al [69] observed a polarization dependence almost solely given by the dielectric contrast for wurtzite CdSe nanowires. Mishra et al. [35] observed a polarization dependence for InP nanowires dominated by the selection rules of the optical transitions, so that the polarization of the emitted light was perpendicular to the nanowires, but with a fairly low polarization ratio, since the difference in dielectric constant still play a role.

For the measurements discussed in Paper III, the dominating effect is the difference in dielectric constants, and the photocurrent was largest for excitation light polarized parallel to the nanowire. The nanowires in this study have very little tapering, a fairly large aspect ratio (the length is 3 μm and the diameter is 85 nm) and the wavelength is clearly larger than the nanowire diameter ($\lambda > 1\,\mu$m). However, the fact that the nanowire is of wurtzite crystal structure can be one reason for the low measured polarization ratio compared to the what can be expected from the difference in dielectric

constant between the nanowire and its surroundings. It should, however, not affect the measured photocurrent onset too much. The absorption will be weaker than for a zinc blende structure, since the light that is strongly absorbed due to the selection rules is attenuated due to the dielectric contrast. It is however not zero, and in addition, the selection rule is only strict at $\mathbf{k}$=0, and further out in k-space, it is a less rigorous selection rule due to band mixing.

Chapter 6

Single molecule spectroscopy of the conjugated polymer MEH-PPV

In this chapter single chains of the conjugated polymer MEH-PPV are studied with PL spectroscopy at room temperature and at 20 K to investigate the conformational changes of the polymer. The chapter starts with a brief introduction to conjugated polymers.

6.1 Conjugated polymers

The term conjugated polymer refers to a class of organic polymers, or plastic, where the bonds between the carbon atoms in the polymer backbone are alternating double and single bonds, Figure 6.1. This structure gives the polymers optical and electrical properties that makes them interesting for use in for example light emitting diodes, displays and solar cells [72–74]. It is attractive to make such devices from plastic because there are techniques to process the material to thin and large area films from solution, and the polymer film can be deposited on low cost substrates [75]. In addition, plastic is mechanically flexible, which could be interesting for displays and solar cells. Also, the optical properties of the polymer can be tuned by changing its chemical structure, and the side chains. One important and well investigated class of polymers for optical applications is the PPV:s (poly (para phenylene vinylene)) and in this thesis the polymer MEH-PPV
poly[2-methoxy-5-(2'-ethyl-hexyloxy)-1,4-phenylene vinylene] is studied.

The concept of conjugation is illustrated in Figure 6.1. In a conjugated polymer all the carbon atoms in the polymer backbone are sp^2 hybridized.

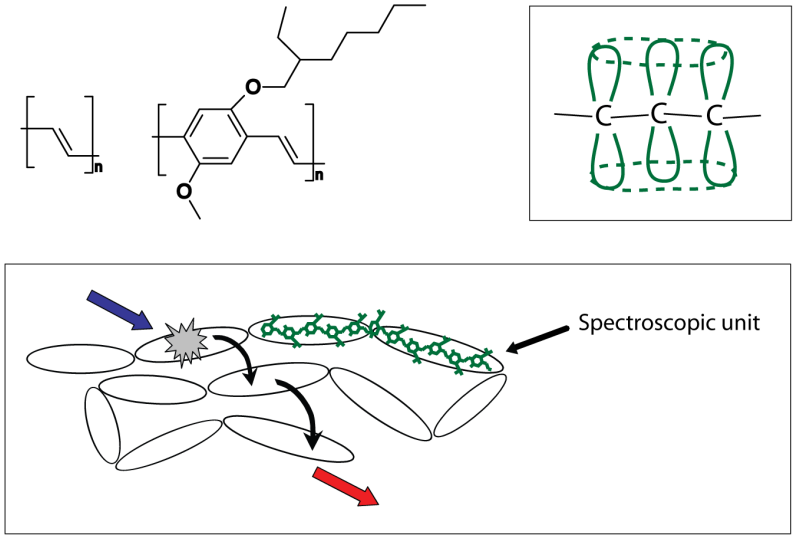

Figure 6.1: The backbone of a conjugated polymer consist of alternating double and single bonds. Shown in the upper left corner of the figure are monomers of two such polymers. To the left is the simplest conjugated polymer, polyacetylene. To the right is a monomer of MEH-PPV, the polymer studied in this thesis. For MEH-PPV the conjugation is over the benzene ring. In the upper right corner the concept of π-conjugation is shown. Sigma bonds are marked as black lines, and the bonds oriented perpendicular to the plane of the paper are omitted for clarity. The p-orbitals are the gray solid lines, and the sharing of electrons are illustrated with dashed lines. In the lower half of the figure the excitation energy transport between spectroscopic units is illustrated.

This means that three of the four valence electrons are in three equivalent orbitals that are a mix of one s-orbital and two p-orbitals. These orbitals are part of the single bonds to the nearest atoms (the σ-bonds). The remaining valence electron is in a p-orbital. This orbital can overlap with the p-orbitals on the neighbouring carbon atoms, forming a delocalized π-orbital. The electrons in these orbitals can delocalize over long distances on the polymer backbone. A large number of these interacting delocalized electrons lead to something similar to a band structure with a band gap corresponding to visible light. Thus the polymer chain is in some sense a one-dimensional semiconductor.

However, the polymer will not be a straight chain, but bent in various shapes due to the environment or defects in the polymer, such as single bonds. This limits the delocalization of the electrons and the polymer is divided into short segments, about 10 monomers in length, of unbroken conjugation, and that will affect the optical properties of the polymer. The optical excitation is localized on short segments of the polymer chain, called spectroscopic units or chromophores. The length of these units is not necessarily equal to the distance between two defects [76]. All the spectroscopic units can absorb the excitation light, and the excitation energy is then transferred between the spectroscopic units until it reaches a local energy minimum, that is a spectroscopic unit with low emission energy. As the excitation is transferred between the spectroscopic units some of the energy is lost, and once at the local energy minimum the excitation can travel no further and the spectroscopic unit emits light [77]. This is illustrated in Figure 6.1. How far the excitation can travel, and thereby the number of emitting sites, is controlled by the distance between the spectroscopic units and their relative orientation, and thus by how the polymer chain is folded. The way the polymer is folded is termed conformation. The conformation is controlled by the chemical structure of the polymer chain, the number and type of defects on the polymer chain [78], charges on or in the vicinity of the polymer chain and the surroundings, such as the choice of host matrix [79]. One effect of this is that the conformation of the polymer is sensitive to the choice of solvent [80, 88]. It has also been shown that the conformation the polymer had in the solution is to some extent retained in a film spin-coated from the solution [81]. However, if the film is annealed the conformation becomes independent of the choice of solvent [82].

In this thesis MEH-PPV is studied dispersed in a host matrix spun cast from a toluene solution. With this choice of solvent, the MEH-PPV has a conformation with closely packed chains, called defect cylinder [78]. The chains are so closely packed, that the efficient energy transfer results in emis-

sion from a few spectroscopic units, or even a single spectroscopic unit. The polymer therefore behaves as a single emitter despite its large size. Effects of this can be seen in the form of blinking in the PL [83], i.e. the polymer stops emitting light during short periods of time. However, as discussed in [84], the energy transfer is perhaps not necessary to explain the blinking effect. The most convincing proof that a polymer chain spun-cast from a toluene solution emits from only a few sites, is that photon cross correlation spectroscopy has shown that the light emission is anti-bunched [85], and in that work, the upper limit of the number of emitting sites was estimated to 2–3.

6.1.1 Single molecule spectroscopy of conjugated polymers

The PL measurements described in this thesis are made on individual polymer chains. This enables the study of the conformation of an individual chain without ensemble averaging, and as will be apparent from the discussion of the results, the polymer chains can take on a large number of conformations with different emission energies, and these conformations can vary with time. These effects can not be distinguished in an ensemble measurement. Another reason to study single polymer chains is that in a film the polymer chains can interact, and this interaction is affected by the film morphology. Also the excitation is no longer only localized to a single spectroscopic unit, but the nearby chains open up the possibilities for more delocalized low energy excitation species [81]. All these complications are avoided when studying single polymer chains. Of course, in order to make optimized devices it is also necessary to study the polymer films. This is, however, beyond the scope of this thesis.

6.2 Experimental details

The polymer, MEH-PPV, synthesized as in [86], has a high molecular weight average $M_w > 1500000$ g/mol and a polydispersity of 2. The polymer contains almost 5000 monomers, which corresponds to some 600 spectroscopic units. A toluene solution of MEH-PPV and PMMA (the host matrix) was spun cast onto a Si substrate. This resulted in sample with a film thickness of about 50 nm. The MEH-PPV chains were separated by about 20 μm in the film plane. The sample was placed in the cold-finger cryostat and a vacuum better than 10^{-5} mbar was kept for more than 10 hours to remove oxygen from the film, and thereby reduce the photobleaching caused by oxygen. The

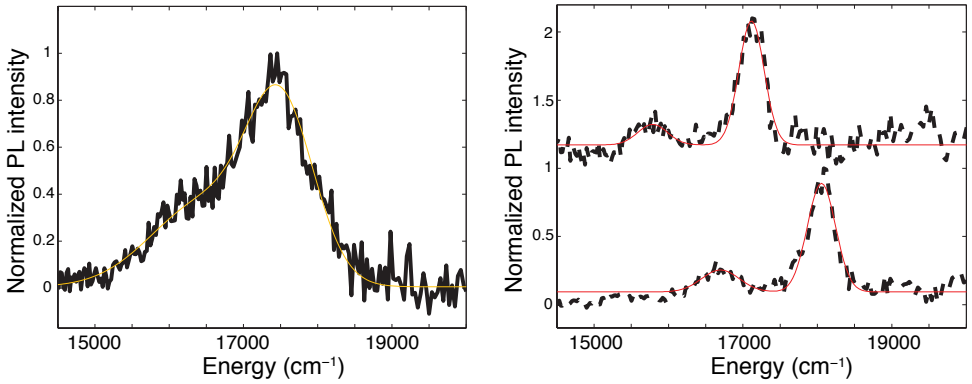

Figure 6.2: Left: PL spectrum of a single MEH-PPV chain acquired at room temperature. Right: spectra from two single MEH-PPV chains at 20 K. For all spectra the acquisition time was 90 s. The solid red line is a fit of Equation 6.1 to the data.

sample was studied in the cryostat at room temperature and at about 20 K. The measurements were performed in the setup described in Section 2.1. Further detail on the sample preparation can be found in Paper I and [87].

6.3 Temperature dependent conformational dynamics in MEH-PPV

Figure 6.2 shows the PL spectrum from a single MEH-PPV chain at room temperature. The acquisition time was 90 s. Assuming that the spectral shape corresponded to two vibronic peaks, the spectra were fitted with a sum of two Gaussian peaks according to Equation 6.1. y_0 is an offset, A_{00} (A_{01}) is the amplitude of the first (second) peak, w_{00} (w_{01}) is the width of the first (second) peak, ν is the energy and ν_{00} (ν_{01}) is the PL peak position. Figure 6.3 shows the distribution of fitted peak positions for 57 single MEH-PPV chains. Note that the width of the distribution is of the same size as the average spectral width of the first peak.

$$\begin{aligned} y &= y_0 + \frac{A_{00}}{w_{00}\sqrt{\pi/2}} \exp\left(-2\left(\frac{\nu-\nu_{00}}{w_{00}}\right)^2\right) \\ &\quad + \frac{A_{01}}{w_{01}\sqrt{\pi/2}} \exp\left(-2\left(\frac{\nu-\nu_{01}}{w_{01}}\right)^2\right) \end{aligned} \tag{6.1}$$

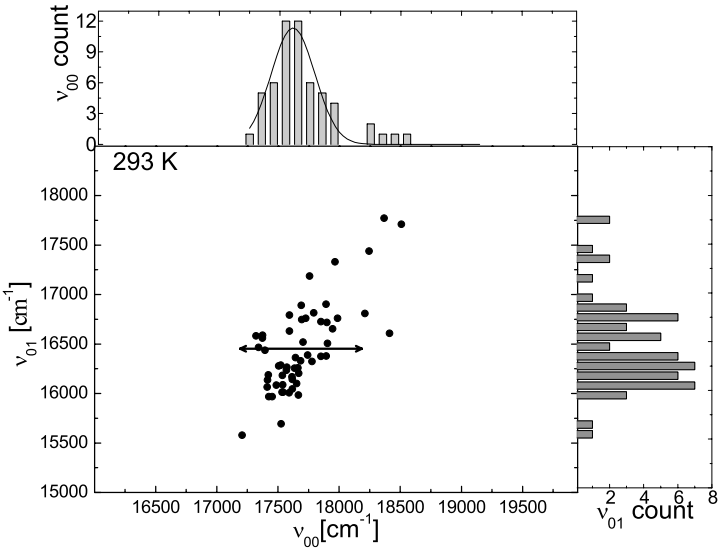

Figure 6.3: The peak position of the first vibronic peak plotted versus the position of the second peak (parameters ν_{00} and ν_{01} respectively) for 57 single MEH-PPV chains. Room temperature. The double arrow indicates the average width of the first vibronic peak (w_{00}). The figure is taken from Paper I.

The average separation between the first and second PL peak was 1236 cm^{-1}, in reasonable agreement with the vibrational frequency for the stretching of the polymer backbone. The width of the spectra acquired at room temperature with an integration time of 90 s were somewhat broader and less structured than typical spectra found in literature where the integration time is a few seconds, see for example [88]. More importantly, there was hardly any spectral evolution as measured by comparing spectra acquired with 45 s, 90 s and 180 s integration time, respectively. The spectra are wide enough to be explained by that during the 90 s integration time, we have averaged over all the possible emission spectra for that particular polymer chain, and that would also explain the lack of spectral evolution.

There were, however, intensity changes with time. Both smaller intensity fluctuations and complete on-off blinking was observed at room temperature as well as at 70 K. Since this was not further investigated, it is not discussed in Paper I.

The spectra of two individual polymer chains at 20 K are shown in Figure 6.2. The spectra were narrower and the two vibronic peaks were more pronounced than at room temperature. A number of chains showed one, three or four peaks. These multipeaked spectra were attributed to polymers

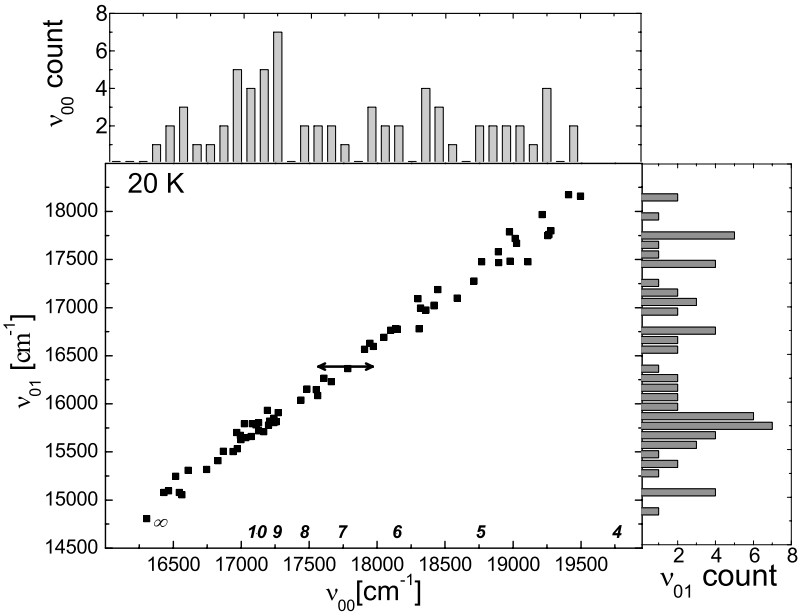

Figure 6.4: The position of the first vibronic peak plotted versus the position of the second peak (parameters ν_{00} and ν_{01} respectively) for 68 single MEH-PPV chains. The temperature is 20 K. The double arrow indicates the average width of the first vibronic peak (w_{00}). The labels at the lower axis are placed at the emission wavenumber of an oligomer of the length indicated by the label. The figure is taken from Paper I.

with multiple emitting sites, and were left out of the analysis. The average width of the first vibronic peak for 68 single chains was 398 cm^{-1}. Even narrower spectral line widths, zero phonon lines with a width of 20 cm^{-1}, were seen by [89]. They also observed an additional vibronic progression. More recently, [90] reported emission linewidths of less than 3 cm^{-1}. In [89] the larger line width in Paper I (and [91]) is attributed to for example simultaneous emission from multiple chromophores or aggregation, and [90] suggest that rapid spectral diffusion is present already at temperatures as low as 20 K.

What is actually more surprising than the narrowing of the spectra at low temperature is the distribution of the spectral peaks, Figure 6.4. The spectra were spread over more than 3000 cm^{-1}, almost ten times the spectral width. At room temperature the spread was comparable to the spectral width.

The spectral evolution at 20 K was measured for 20 of the polymer chains by acquiring consecutive spectra of the same polymer chain. At this low temperature the photobleaching is reduced, and the polymer chains could

be observed during several tens of minutes. 11 of the molecules exhibited shifts of less than 60 cm^{-1}, which was the smallest shift that could be clearly distinguished with the signal to noise ratio in the measurement. The other 9 shifted between 60 cm^{-1} and 420 cm^{-1} during the observation time. These shifts are clearly smaller than the spread in the spectral maxima. The spectra shifted to the red as well as to the blue, which indicates that the shifts were not exclusively caused by photobleaching, which would cause a blueshift of the spectrum as the lowest emitting site is destroyed, see for example [88]. We attributed these shifts to small conformational rearrangements of the polymer chain. References [92] and [93] showed a spectral diffusion over a larger range for MEH-PPV dispersed on a surface and covered by a PVA cap, allowing for easier conformational rearrangement of the polymer.

The interpretation of the results are as follows: The polymer can take on a large number of conformations. The changes between different conformations could take place by torsional motions in the polymer, resulting in changes in the length of the emitting spectroscopic unit. At room temperature the available thermal energy is large enough to allow the polymer chain to sample most of the conformations on the timescale of the acquisition time (90s), resulting in a broad spectrum with virtually no spectral evolution and only small differences in the position of the spectral maxima among individual chains. At 20 K, however, the available thermal energy is only 15 cm^{-1} and thus the conformation of the polymer is frozen, resulting in a narrow spectrum. Each individual polymer chain is stuck in one of the many possible conformations, leading to a wide distribution of spectral maxima among the chains. Estimations of the emission energy of a spectroscopic unit of a specific length (see Paper I for details) showed that the entire range of observed emission frequencies can be covered if the emitting sites have between 4 and infinitely many monomers in the spectroscopic unit.

Summary of the papers

My contributions to the papers are specified below for each paper. For all papers I took part in the data analysis, and for all papers I took part in writing the paper, and for the papers where I am the first author I wrote the paper. I have not done the epitaxial growth of the nanowires, but I have taken part in the discussions on how to optimize the growth for improving the optical properties of the nanowires.

I. Temperature effect on single chain MEH-PPV spectra
C. Rønne, J. Trägårdh, D. Hessman, V. Sundström
Chem. Phys. Lett. **388**, 40 (2004)

In this paper, a study of the conformations of the conjugated polymer MEH-PPV (poly[2-methoxy-5-(20 -ethyl-hexyloxy)-1,4-phenylene vinylene]) embedded in a PMMA matrix, using single molecule photoluminescence spectroscopy was presented. We compared the photoluminescence spectra acquired at room temperature and at 20 K using integration times of 90 s. We observed that at room temperature spectra from different individual polymer chains are very similar, whereas at 20 K the spectrum from a single chain consisted of a few narrow peaks and the emission from individual chains was spread over 3000 cm^{-1}. We proposed that at room temperature fluctuations of conformations with distinct emission properties cause broadening of the spectra and reduce the differences in photoluminescence spectra between individual chains. At 20 K, however, each individual polymer chain is frozen in a specific conformation. This was the first paper presenting narrow low temperature spectra on single MEH-PPV chains.

I prepared the samples and performed the spectroscopy on the single polymer chains.

II. Growth and optical properties of strained GaAs-$Ga_xIn_{1-x}P$ core-shell nanowires

N. Sköld, L.S. Karlsson, M.W. Larsson, M-E Pistol, W. Seifert, J. Trägårdh, L. Samuelson
Nano Letters **5**, 1943 (2005)

In this paper we studied photoluminescence of GaAs-$Ga_xIn_{1-x}P$ ($0.34 < x < 0.69$) core-shell nanowires grown by metal-organic vapor phase epitaxy. Photoluminescence measurements on individual nanowires at 5 K showed that the emission efficiency increased by 2 to 3 orders of magnitude compared to uncapped samples. Strain effects on the band gap of lattice mismatched core-shell nanowires were studied and confirmed by calculations based on deformation potential theory. We also showed, using time-resolved photoluminescence, that the transport of charge carriers from the shell to the core is partially hindered at low temperatures such as 5 K. This was the first paper to present core-shell nanowires where the strain was tuned by a ternary shell.

I performed the time-resolved photoluminescence measurements.

III. Infrared Photodetectors in Heterostructure Nanowires

H. Pettersson, J. Trägårdh, A.I. Persson, L. Landin, D. Hessman, L. Samuelson
Nano Letters **6**, 229 (2006)

We performed spectrally resolved photocurrent measurements on single InAs nanowires with a centrally placed $InAs_{1-x}P_x$ segment. The nanowires were contacted at the InAs ends of the nanowire. The conduction band offset between the InAs and $InAs_{1-x}P_x$ regions virtually removed the dark current through the wires at low temperature of up to 77K. The photocurrent onset was in qualitative agreement with the expected band gap of the $InAs_{1-x}P_x$ segment composition. Furthermore, we observed a strong polarization dependence in the photocurrent, due to the dielectric contrast between the nanowire and its surroundings. This is one of the few papers presenting *spectrally resolved* photocurrent measurements on III-V nanowires.

I prepared the samples and performed most of the photocurrent measurement.

IV. Measurements of the band gap of wurtzite $InAs_{1-x}P_x$ nanowires using photocurrent spectroscopy
J. Trägårdh, A.I. Persson, J.B. Wagner, D. Hessman, L. Samuelson
Journal of Applied physics **101**, 123701 (2007)

In this paper we measured the band gap of $InAs_{1-x}P_x$ nanowires having wurtzite crystal structure as a function of the composition for $0.14 < x < 0.48$. The band gap was measured by photocurrent spectroscopy on single InAs nanowires with a centrally placed $InAs_{1-x}P_x$ segment. The obtained band gaps were larger than the corresponding zinc blende band gaps by about 120 meV over the entire composition range. We attribute this increase to the fact that the crystal structure was wurtzite rather than zinc blende. The strength of this paper is that it uses an absorption-type measurement technique, rather than photoluminescence measurements, to investigate the band gap of nanowires with wurtzite crystal structure.

I prepared the samples and performed the photocurrent measurements.

V. Optical Properties of Rotationally Twinned InP Nanowires
J. Bao, D. C. Bell, F. Capasso, J. B. Wagner, T. Mårtensson, J. Trägårdh and L. Samuelson
Nano Letters **8** 836 (2008)

Using a special TEM grid, that was developed for this study, transmission electron microscopy and photoluminescence spectroscopy were performed on the same single nanowire. We could thereby correlate structural and optical properties of a rotationally twinned zinc blende InP nanowire and a twin-free InP nanowire. We also performed photoluminescence spectroscopy on a larger number of the InP nanowires spread out on an ordinary substrate. An excitation power dependent blue-shift of the photoluminescence was observed for the InP nanowires with rotational twins but not for the twin-free nanowires. We proposed that this effect was due to that in the rotationally twinned nanowire, the type II offset between zinc blende InP and wurtzite InP leads to that the holes localize in wurtzite-like regions with a high density of twins and the electrons localize in the more zinc blende-like regions with a low density of twins.

I took part in the photoluminescence measurement not combined with TEM, and in the discussions related to the understanding of the physics of the system.

VI. Monolithic GaAs/InGaP nanowire LEDs on silicon
P. Svensson, T. Mårtensson, J. Trägårdh, C. Larsson, M. Rask, D. Hessman, L. Samuelson, J. Ohlsson
Submitted to Nanotechnology (2008)

In this paper we demonstrated fabrication of vertical light-emitting diodes based on GaAs-GaInP core-shell nanowires, epitaxially grown on GaP and Si substrates. This was the first demonstration of nanowire-based LEDs manufactured using planar processing techniques. LED functionality was established on both kinds of substrates and the devices were evaluated in terms of temperature-dependent photoluminescence and electroluminescence.

I performed the photoluminescence spectroscopy.

VII. Gate-dependent photoluminescence from single *p*- and *n*-doped InP nanowires
J. Trägårdh, D. Hessman, M.T. Borgström, E. Norberg and L. Samuelson
Manuscript (2008)

We investigated p- and n-doped InP nanowires with photoluminescence (PL) spectroscopy on individual nanowires. The Fermi level pinning at the surface induces a radial band bending in the nanowires, since the donors or acceptors can form a space charge. This band bending results in a lowering of the PL energy. We showed that the peak-position of the PL could be tuned by applying a gate voltage to the nanowire, as well as by increasing the excitation power. We attribute the change in PL energy to a change in band bending. This could potentially be used to investigate the doping concentration in nanowires.

I performed the photoluminescence spectroscopy.

Populärvetenskaplig sammanfattning

I den här avhandlingen används ljus för att studera egenskaper hos nanotrådar av halvledarmaterial.

Nanotrådarna har en tjocklek som är 100 nm eller mindre, och en längd som är minst tio gånger större (1 nm = 1/1000000000 m. Som jämförelse är ett hårstrå tusen gånger tjockare än en nanotråd). Föremål på den här skalan har en mycket stor yta i förhållande till den volym de upptar, vilket gör att nanotråden är väldigt känslig för vad som pågår på ytan. För sensorer där ytan är den aktiva delen är det en tillgång, men för nanometer-stora lysdioder eller lasrar kan den stora ytan istället bli ett problem. På ytan finns nämligen extra energitillstånd, och en elektron som är nära ytan (vilket varenda elektron i en nanotråd är eftersom nanotråden är så tunn) kan använda dessa tillstånd för att minska sin energi, istället för att skicka ut en foton. Den energi som tillförts lysdioden eller lasern förloras därmed till stor del i form av värme, och är därmed bortslösad.

Ett sätt att lösa problemet är att täcka ytan med ett material som gör att elektronerna hålls borta från den yttersta ytan och stannar i mitten på nanotråden. Sådana strukturer kallas core-shell (kärna-skal) nanotrådar. I den här avhandlingen har sådana nanotrådar studerats med en metod som kallas tidsupplöst fotoluminescens, där man mäter hur många fotoner som sänds ut från nanotråden beroende på hur lång tid (på skalan av en miljarddels sekund) det gått sedan man tillförde energi till elektronerna med en kort laserpuls. I medeltal tar det mycket längre tid för en elektron att förlora energi genom att skicka ut en foton än att förlora energin som värme med hjälp av ett energitillstånd på ytan. Avklingningstiden för det utsända ljuset ger därmed ett mått på hur många tillstånd det finns kvar på ytan där elektronen kan förlora sin energi, och därmed ett mått på hur väl skalet på nanotråden fungerar.

För den sortens halvledarmaterial som studeras här finns det två olika sätt att stapla atomerna för att skapa en kristall. De två möjliga kristallstrukturerna kallas zincblende och wurtzite. I materialbitar av större storlek observerar man bara zincblende-strukturen, medan nanotrådar kan ha bägge

kristallstrukturerna. De två kristallstrukturerna har lite olika egenskaper även när det är samma atomer som bygger upp materialet; De har till exempel olika bandgap, och absorberar därför ljus av olika våglängd, och elektronens effektiva massa är olika. För att kunna använda nanotrådarna i komponenter måste man känna till dessa egenskaper även för wurtzite-strukturen (och eftersom den inte finns i bulk har man inte mätt egenskaperna tidigare). I avhandlingen har bandgapet för nanotrådar med wurtzite-struktur studerats för ett antal sammansättningar av en legering mellan indium (In) arsenik (As) och fosfor (P). Metoden som används är fotoströmsspektroskopi. Små elektriska kontakter till nanotråden tillverkas med hjälp av elektronstråle-litografi, och sedan mäts strömmen när vi lyser på nanotråden med ljus med olika färg och därmed olika energi. Ljuset ger elektronerna energi, och får de tillräckligt mycket energi börjar nanotråden leda ström. Den energi som behövs är bandgapsenergi. Nanotråden fungerar faktiskt som en mycket liten fotodetektor för infrarött ljus.

En mindre del av avhandlingen handlar om att, också här med hjälp av ljus, studera egenskaperna hos en speciell typ av plastmaterial som kan absorbera och sända ut synligt ljus samt leda ström. (Vanlig plast är normalt elektriskt isolerande och färglöst, dvs kan inte växelverka med synligt ljus.) Dessa egenskaper hos plasten gör att man skulle kunna använda plasten i t.ex. lysdioder och solceller. En fördel med plast jämfört med de halvledarmaterial man brukar göra t.ex. lysdioder av, är att plast är flexibelt och kan formas till nästan vilken form som helst, eller valsas ut till en tunn film. Framförallt finns det billiga processningsmetoder för att tillverka och forma plast. Plast är polymerer, dvs. långa kedjor av molekyler, och den här sortens plast kallas konjugerade polymerer. Speciellt har formen på polymeren, dvs hur den viker ihop sig studerats. Genom sänka temperaturen i polymerens omgivning till $-253°$C så fixerar man den form polymeren har. Den kan inte få värmeenergi nog att ändra sin form. Spektrumet för det utsända ljuset från polymeren ger en bild av hur just den polymerkedjan är ihopvikt. Genom att mäta på många polymerkedjor kan man se vilka möjliga sätt det finns för polymeren att vika ihop sig på. Genom att jämföra med samma mätningar vid rumstemperatur, där polymeren kan ändra sin form, kan man dra slutsatser om hur polymeren gör för att vika om sig.

References

[1] T. Kuykendall, P. Ulrich, S. Aloni, and P. Yang, *Complete composition tunability of InGaN nanowires using a combinatorial approach*, Nature Materials **6**, 951 (2007)

[2] A.I. Persson, M.T. Björk, S. Jeppesen, J.B. Wagner, L.R. Wallenberg, and L. Samuelson, *InAs1-xPx nanowires for device engineering*, Nano Lett. **6**, 403 (2006)

[3] M.T. Björk, B.J. Ohlsson, T. Sass, A.I. Persson, C. Thelander, M.H. Magnusson, K. Deppert, L.R. Wallenberg, and L. Samuelson, *One-dimensional steeplechase for electrons realized*, Nano. Lett. **2**, 87 (2002)

[4] Y. Wu, R. Fan, and P. Yang, *Block-by-block growth of single crystalline Si/SiGe superlattice nanowires*, Nano Lett. **2**, 83 (2002)

[5] M.S. Gudiksen, L.J. Lauhon, J. Wang, D.C. Smith, and C.M. Lieber, *Growth of nanowire superlattice structures for nanoscale photonics and electronics*, Nature **415**, 617 (2002)

[6] E. Ertekin, P.A. Greaney, D.C. Chrzan, and T.D. Sands, *Equilibrium limits of coherency in strained nanowire heterostructures*, J. Appl. Phys. **97**, 114325 (2005)

[7] M.G. Lagally and R.H. Blick, *Materials science: A 'bed of nails' on silicon*, Nature **432** 450 (2004)

[8] T. Mårtensson, C.P.T. Svensson, B.A. Wacaser, M.W. Larsson, W. Seifert, K. Deppert, A. Gustafsson, L.R. Wallenberg, and L. Samuelson, *Epitaxial III-V nanowires on silicon*, Nano Lett. **4**, 1987 (2004)

[9] S.G. Ihn, J.I. Song, Y.H. Kim, J.Y. Lee, and I.H. Ahn, *Growth of GaAs Nanowires on Si Substrates Using a Molecular Beam Epitaxy*, IEEE Transactions on Nanotechnology **6**, 384 (2007)

[10] M. Danek, K.F. Jensen, C.B. Murray, and M.G. Bawendi, *Synthesis of Luminescent Thin-Film CdSe/ZnSe Quantum dot composites using CdSe quantum dots passivated with an overlayer of ZnSe*, Chem. Mater. **8**, 173 (1996)

[11] J. Noborisaka, J. Motohisa, S. Hara, and T. Fukui, *Fabrication and characterization of freestanding GaAs/AlGaAs core-shell nanowires and AlGaAs nanotubes by using selective-area metalorganic vapor phase epitaxy*, Appl. Phys. Lett. **87**, 093109 (2005)

[12] L.V. Titova, T.B. Hoang, H.E. Jackson, L.M. Smith, J.M. Yarrison-Rice, Y. Kim, H.J. Joyce, Q. Gao, H.H. Tan, and C. Jagadish, *Temperature dependence of photoluminescence from single core-shell GaAs-AlGaAs nanowires*, Appl. Phys. Lett. **89**, 173126 (2006)

[13] F. Qian, S. Gradeak, Y. Li, C-Y. Wen and C. M. Lieber, *Core/Multishell Nanowire Heterostructures as Multicolor, High-Efficiency Light-Emitting Diodes*, Nano Lett. **5**, 2287 (2005)

[14] O. Hayden, A. B. Greytak, and D. C. Bell, *Core-Shell Nanowire Light-Emitting Diodes*, Adv. Mater. **17**, 701 (2005)

[15] J. Xiang, W. Lu, Y.J. Hu, Y. Wu, H. Yan, and C.M. Lieber, *Ge/Si nanowire heterostructures as high-performance field-effect transistors*, Nature **441**, 489 (2006)

[16] X.C. Jiang, Q.H. Xiong, S. Nam, F. Qian, Y. Li, and C.M. Lieber, *InAs/InP radial nanowire heterostructures as high electron mobility devices*, Nano Lett. **7**, 3214 (2007)

[17] J. Johansson, B.A. Wacaser, K.A. Dick, and W. Seifert, *Growth related aspects of epitaxial nanowires*, Nanotechnology **17**, S355 (2006)

[18] E.F. Schubert, *Light-emitting diodes* p. 28 (Cambridge University Press, Cambridge 2006) ISBN 978-0-521-86538-8

[19] R.K. Ahrenkiel, *Measurements of the minority-carrier lifetime by time-resolved photoluminescence*, Solid State Electronics **35**, 239 (1992)

[20] M. T. Björk, C. Thelander, A. E. Hansen L. E. Jensen, M. W. Larsson, L. R. Wallenberg, and L. Samuelson, *Few-electron quantum dots in nanowires*, Nano Lett. **4**, 1621 (2004)

[21] A.I. Persson, L.E. Fröberg, S. Jeppesen, M.T. Björk, and L. Samuelson, *Surface diffusion effects on growth of nanowires by chemical beam epitaxy*, J. Appl. Phys. **101**, 034313 (2007)

[22] N. Sköld, J.B. Wagner, G. Karlsson, T. Hernán, W. Seifert, M-E. Pistol, and L. Samuelson, *Phase segregation in AlInP shells on GaAs nanowires*, Nano Lett. **6**, 2743 (2006)

[23] K.A. Dick, S. Kodambaka, M.C. Reuter, K. Deppert, L. Samuelson, W. Seifert, L.R. Wallenberg, and F.M. Ross, *The Morphology of Axial and Branched Nanowire Heterostructures*, Nano Lett. **7**, 1817 (2007).

[24] K.A. Dick, K. Deppert, L.S. Karlsson, L.R. Wallenberg, L. Samuelson, and W. Seifert, *A new understanding of Au-assisted growth of III-V semiconductor nanowires*, Adv. Funct. Mater. **15**, 1603 (2005)

[25] J. Eriksson, *Cross-sectional scanning tunneling microscopy of III-V semiconductor nanowires*, licentiate thesis, Lund University (2008)

[26] C. Thelander, M. T. Björk, M. W. Larsson, A. E. Hansen, L. R. Wallenberg, and L. Samuelson, *Electron transport in InAs nanowires and heterostructure nanowire devices*, Solid State Commun. **131**, 573 (2004)

[27] M. T. Borgström, E. Norberg, P. Wickert, H. Nilsson, J. Trägårdh, K. Dick, G. Statkute, P. Ramvall, K. Deppert, and L. Samuelson, *Precursor evaluation for in-situ InP nanowire doping*, To be published

[28] Aspnes D.E., *Recombination at semiconductor surfaces and interfaces*, Surface Science **132**, 406-421 (1983)

[29] D.W. Wang, Y.L. Chang, Q. Wang, J. Cao, D.B. Farmer, R.G. Gordon, and H.J. Dai, *Surface Chemistry and Electrical Properties of Germanium Nanowires*, J. Am. Chem. Soc. **126**, 11602 (2004)

[30] I. Kimukin, M.S. Islam, and R.S. Williams, *Surface depletion thickness of p-doped silicon nanowires grown using metal-catalysed chemical vapour deposition*, Nanotechnology **17**, S240 (2006)

[31] M.H.M. van Weert, O. Wunnicke, A.L. Roest, T.J. Eijkemans, A. Yu Silov, J.E.M. Haverkort, G.W. 't Hooft, and E.P.A.M. Bakkers, *Large redshift in photoluminescence of p-doped InP nanowires induced by Fermi-level pinning*, Appl. Phys. Lett. **88**, 043109 (2006)

[32] K. Ogawa, K. Haraguchi, K. Hiruma, Y. Fujisaki, T. Katsuyama, and G. Fasol, *Spectral and temporal features of photoluminescence of gallium arsenide quantum-wire crystals*, J. Lumin. **53**, 387 (1992)

[33] E. Yablonovitch, C.J. Sandroff, R. Bath, and T. Gmitter, *Nearly ideal electronic properties of sulfide coated GaAs surfaces*, Appl. Phys. Lett. **51**, 439 (1997)

[34] M. Mattila, T. Hakkarainen, M. Mulot, and H. Lipsanen, *Crystal-structure-dependent photoluminescence from InP nanowires*, Nanotechnology **17**, 1580 (2006)

[35] A. Mishra, L.V. Titova, T.B. Hoang, H.E. Jackson, L.M. Smith, J.M. Yarrison-Rice, Y. Kim, H.J. Joyce, H.H. Tan, and C. Jagadish, *Polarization and temperature dependence of photoluminescence from zincblende and wurtzite InP nanowires*, Appl. Phys. Lett. **91**, 263104 (2007)

[36] C. Chen, N. Braidy, C. Couteau, C. Fradin, G. Weihs and R. LaPierre, *Multiple quantum well AlGaAs nanowires*, Nano Lett. **8**, 495 (2008)

[37] P. Mohan, J. Motohisa, and T. Fukui, *Fabrication of InP/InAs/InP core-multishell heterostructure nanowires by selective area metalorganic vapor phase epitaxy*, Appl. Phys. Lett. **88**, 133105 (2006)

[38] H.J. Choi, J.C. Johnson, R. He, S-K. Lee, F. Kim, P. Pauzauskie, J. Goldberger, R.J. Saykally, and P. Yang, *Self-organized GaN quantum wire UV lasers*, J. Phys. Chem. B **107**, 8721 (2003)

[39] Z. Zanolli, L.E. Fröberg, M.T. Björk, M-E. Pistol, and L. Samuelson, *Fabrication, optical characterization and modeling of strained core-shell nanowires*, Thin Solid Films **515**, 793 (2006)

[40] H.J. Joyce, Q. Gao, H.H. Tan, C. Jagadish, Y. Kim, X. Zhang, Y.N. Guo, and J. Zou, *Twin-free uniform epitaxial GaAs nanowires grown by a two-temperature process*, Nano Lett. **7**, 921 (2007)

[41] E.P. O'Reilly and A.R. Adams, *Band-Structure Engineering in Strained Semiconductor Lasers*, IEEE J. Quantum Electron. **30**, 366 (1994)

[42] H.E. Ruda and A. Shik, *Polarization sensitive phenomena in semiconducting and metallic nanowires*, Phys. Rev. B **72**, 115308 (2005)

[43] D.J. Sirbuly, M. Law, H. Yan, and P. Yang, *Semiconductor Nanowires for Subwavelength Photonics Integration*, J. Phys. Chem. B **109**, 15190 (2005)

[44] W. Seifert, M. Borgström, K. Deppert, K. Dick, J. Johansson, M.W. Larsson, T. Mårtensson, N. Sköld, C.P.T. Svensson, B.A. Wacaser, L.R. Wallenberg, and L.Samuelson, *Growth of one-dimensional nanostructures in MOVPE*, J. Cryst. Growth **272**, 211 (2004)

[45] K. Hiruma, M. Yazawa, K. Haraguchi, K. Ogawa, T. Katsuyama, M. Koguchi, H. Kakibayashi *GaAs free-standing quantum-size wires*, J. Appl. Phys. **74**, 3162 (1993)

[46] F. Martelli, M. Piccin, G. Bais, F. Jabeen, S. Ambrosini, S. Rubini, and A. Franciosi, *Photoluminescence of Mn-catalyzed GaAs nanowires grown by molecular beam epitaxy*, Nanotechnology **18**, 125603 (2007)

[47] P. Mohan, J. Motohisa, and T. Fukui, *Controlled growth of highly uniform axial/radial direction-defined, individually addressable InP nanowire arrays*, Nanotechnology **16**, 2903 (2005)

[48] C-Y. Yeh, S-H. Wei, and A. Zunger, *Relationships between the band gaps of the zinc-blende and wurtzite modifications of semiconductors*, Phys. Rev. B **50**, 2715 (1994)

[49] J.L. Birman, *Some selection rules for band-band transitions in wurtzite structure*, Phys. Rev. **114**, 1490 (1959)

[50] J. Johansson, L. S. Karlsson, C.P.T. Svensson, T. Mårtensson, B.A. Wacaser, K. Deppert, L. Samuelson, and W. Seifert, *Structural properties of 111B - oriented III–V nanowires*, Nature Materials **5**, 574 (2006)

[51] J. Bauer, V. Gottschalch, H. Paetzelt, G. Wagner, B. Fuhrmann, and H.S. Leipner, *MOVPE growth and real structure of vertical-aligned GaAs nanowires*, J. Cryst. Growth **298**, 625 (2007)

[52] F. Glas, J-C. Harmand, and G. Patriarche, *Why does wurtzite form in nanowires of III-V zinc-blende semiconductors?*, Phys. Rev. Lett. **99**, 146101 (2007)

[53] U. Krishnamachari, M. Borgstrom, B.J. Ohlsson, N. Panev, L. Samuelson, W. Seifert, M.W. Larsson, and L.R. Wallenberg, *Defect-free InP nanowires grown in [001] direction on InP(001)*, Appl. Phys. Lett. **85**, 2077 (2004)

[54] L. Ouattara, A. Mikkelsen, N. Sköld, J. Eriksson, T. Knaapen, E. Cavar, W. Selfert, L. Samuelson, and E. Lundgren, *GaAs/AlGaAs nanowire heterostructures studied by scanning tunneling microscopy*, Nano Lett. **7**, 2859 (2007)

[55] Z. Ikonic, G.P. Srivastava, and J.C. Inkson, *Electronic properties of twin boundaries and twinning superlattices in diamond-type and zinc-blende-type semiconductors*, Phys. Rev. B **48**, 17181 (1993)

[56] Z. Zanolli, F. Fuchs, J. Furthmueller, U. von Barth, and F. Bechstedtet, *Model GW band structure of InAs and GaAs in the wurtzite phase*, Phys. Rev. B **75**, 245121 (2007)

[57] M. Murayama and T. Nakayama, *Chemical trends of band offsets at wurtzite zincblende heterocrystalline semiconductor interfaces*, Phys. Rev. B **49**, 4710 (1994).

[58] I. Vurgaftman and J. R. Meyer, *Band parameters for nitrogen-containing semiconductors*, J. Appl. Phys. **94**, 3675 (2003)

[59] P. Mohan, J. Motohisa, and T. Fukui, *Realization of conductive InAs nanotubes based on lattice-mismatched InP/InAs core-shell nanowires*, Appl. Phys. Lett. **88**, 013110 (2006)

[60] A. Lugstein, A.M. Andrews, M. Steinmair, Y.J. Hyun, E. Bertagnolli, M. Weil, P. Pongratz, M. Schrambock, T. Roch, and G. Strasser, *Growth of branched single-crystalline GaAs whiskers on Si nanowire trunks*, Nanotechnology **18**, 355306 (2007)

[61] M.S. Gudiksen, J. Wang, and C.M. Lieber, *Size-dependent photoluminescence from single indium phosphide nanowires*, J. Phys. Chem. B **106**, 4036 (2002)

[62] Z. Zanolli, M-E. Pistol, L.E. Fröberg, and L. Samuelson, *Quantum-confinement effects in InAs–InP core–shell nanowires*, J. Phys.: Condens. Matter **19**, 295219 (2007)

[63] I. Vurgaftman, J.R. Meyer, and L.R. Ram-Mohan, *Band parameters for III–V compound semiconductors and their alloys*, J. Appl. Phys. **89**, 5815 (2001)

[64] H.X. Lu, P.Y. Yu, L.X. Zheng, S.J. Xu, M.H. Xie, and S.Y. Tong, *Evidence of type II band alignment between cubic and hexagonal phases of GaN*, Appl. Phys. Lett. **82**, 1033 (2003)

[65] T. Bennyattou, M.A. Garica, S. Monéger, A. Tabata, M. Sacilotti, P. Abraham, Y. Monteil, and R. Landers, *Optical characterization of InP/InAlAs/InP interfaces grown by MOVPE*, Appl. Surface Science **63**, 197 (1993)

[66] Q. Liu, S. Derksen, A. Lindner, F. Scheffer, W. Prost, and F-J. Tegude, *Evidence of type-II band alignment at the ordered GaInP to GaAs heterointerface*, J. Appl. Phys. **77**, 1154 (1995)

[67] T.B. Hoang, L.V. Titova, J.M. Yarrison-Rice, H.E. Jackson, A.O. Govorov, Y. Kim , H.J. Joyce, Q. Gao, H.H. Tan, C. Jagadish, and L.M. Smith, *Resonant excitation and imaging of nonequilibrium exciton spins in single core-shell GaAs-AlGaAs nanowires*, Nano Lett. **7**, 588 (2007)

[68] J. Wang, M.S. Gudiksen, X. Duan, Y. Cui, and C.M. Lieber, *Highly polarized photoluminescence and photodetection from single indium phosphide nanowires*, Science **293**, 1455 (2001)

[69] C. X. Shan, Z. Liu, and S. K. Hark, *Photoluminescence polarization in individual CdSe nanowires*, Phys. Rev. B **74**, 153402 (2006)

[70] R.C. Jones, *A generalization of the dielectric ellipsoid problem*, Phys. Rev. **68**, 93 (1945)

[71] J.L. Birman, *Polarization of fluorescence in CdS and ZnS single crystals*, Phys. Rev. Lett. **2**, 157 (1959)

[72] W.U. Huyhn, J.J. Dittmer, and A.P. Alivisatos, *Hybrid nanorod-polymer solar cells*, Science **295**, 2425 (2002)

[73] S.C. Veenstra, J. Loos, and J.M. Kroon, *Nanoscale Structure of Solar Cells Based on Pure Conjugated Polymer Blends*, Prog. Photovolt: Res. Appl. **15**, 727 (2007)

[74] Y. Kim, D.C.C. Bradley, *Bright red emission from single layer polymer light-emitting devices based on blends of regioregular P3HT and F8BT*, Current Appl. Phys. **5**, 222 (2005)

[75] S.R. Forrest, *The path to ubiquitous and low-cost organic electronic appliances on plastic*, Nature **428**, 911 (2004)

[76] J.D. White, J.H. Hsu, W.S. Fann, Shu-Chun Yang, G.Y. Pern, and S.A. Chen, *Deduction of the conformation of short chain luminescent conjugated polymers from single molecule photophysics*, Chem. Phys. Lett. **338**, 263 (2001)

[77] I.G. Scheblykin, A. Yartsev, T. Pullerits, V. Gulbinas, and V. Sundström, *Excited State and Charge Photogeneration Dynamics in Conjugated Polymers*, J. Phys. Chem. B **111**, 6303 (2007)

[78] D. Hu, J. Yu, K. Wong, B. Bagchi, P.J. Rossky, and P.F. Barbara, *Collapse of stiff conjugated polymers with chemical defects into ordered cylindrical conformations*, Nature **405**, 1030 (2000)

[79] S.S. Satori, S. De Feyter, J. Hofkens, M. Van der Auweraer, F. De Schryver, K. Brunner, and J.W. Hofstraat, *Host matrix dependence on the photophysical properties of individual conjugated polymer chains*, Macromolecules **36**, 500 (2003)

[80] T.Q. Nguyen, V. Doan, and B.J. Schwartz, *Conjugated polymer aggregates in solution: Controlling of interchain interactions*, J. Phys. Chem. **110**, 4068 (1999)

[81] B.J. Schwartz, *Conjugated polymers as molecular materials: How chain conformation and film morphology influence energy transfer and interchain interactions*, Annu. Rev. Phys. Chem. **54**, 141 (2003)

[82] T.Q. Nguyen, I.B. Martini, J. Liu, and B.J. Schwartz, *Controlling interchain interactions in conjugated polymers: The effects of chain morphology on exciton–exciton annihilation and aggregation in MEH-PPV films*, J. Phys. Chem. B **104**, 237 (2000)

[83] D.A. Vanden Bout, W. Yip, D. Hu, D. Fu, T.M. Swager, and P.F. Barbara, *Discrete intensity jumps and intramolecular electronic energy transfer in the spectroscopy of single conjugated polymer molecules*, Science **277**, 1074 (1997)

[84] O. Mirzov, F. Cichos, C. von Borczyskowski, and I.G. Scheblykin, *Direct exciton quenching in single molecules of MEH-PPV at 77K*, Chem. Phys. Lett. **386**, 286 (2004)

[85] C.W. Hollars, S.M. Lane, and T. Huser, *Controlled non-classical photon emission from single conjugated polymer molecules*, Chem. Phys. Lett. **370**, 393 (2003)

[86] F.L. Zhang, M. Jonforsen, D.M. Johansson, M.R. Andersson, O. Inganäs, *Photodiodes and solar cells based on the n-type polymer poly(pyridopyrazine vinylene) as electron acceptor*, Synth. Met. **138**, 555 (2003)

[87] J. Trägårdh, *Optical studies of single molecules and single nanowires*, licentiate thesis, Lund University (2006)

[88] T. Huser, M. Yan, and L.J. Rothberg, *Single chain spectroscopy of conformational dependence of conjugated polymer photophysics*, Proc. Nat. Acad. Sci. **97**, 11187 (2000)

[89] F. Schindler, J.M. Lupton, J. Feldmann, and U. Scherf, *A universal picture of chromophore in π-conjugated polymers derived from single-molecule spectroscopy*, Proc. Nat. Acad. Sci. **101**, 14695 (2004)

[90] F.A. Feist, G. Tommaseo, and T. Basché, *Observation of very narrow line widths in the fluorescence excitation spectra of single conjugated polymer chains at 1.2 K*, Phys. Rev. Lett. **98**, 208301 (2007)

[91] Z. Yu and P.F. Barbara, *Low-temperature single molecule spectroscopy of MEH-PPV conjugated polymer molecules*, J. Phys. Chem. B **108**, 11321 (2004)

[92] O. Mirzov, T. Pullerits, F. Cichos, C. von Borczyskowski, and I.G. Scheblykin, *Large spectral diffusion of conjugated polymer single molecule fluorescence at low temperature*, Chem. Phys. Lett. **408**, 317 (2004)

[93] T. Pullerits, O. Mirzov, and I.G. Scheblykin, *Conformational fluctuations and large spectral diffusion in conjugated polymer single chains at low temperature*, J. Phys. Chem. B **109**, 19099 (2005)